Robust two-loop control of the double inverted pendulum

Kamps, E.J.F.

Award date:
1994

EINDHOVEN UNIVERSITY OF TECHNOLOGY
DEPARTMENT OF ELECTRICAL ENGINEERING
Measurement and Control section

Robust two-loop control of the double inverted pendulum

by E.J.F. Kamps

Master of Science Thesis
carried out from December 1993 to December 1994
commisssioned by prof. dr. ir. P. v.d. Bosch
under supervision of dr. ir. A.A.H. Damen
date: December 1993

Summary

Kamps, E.J.F.;
Robust two-loop control of the double inverted pendulum.

In this report a H_∞ design and the two-loop control is applied to the double inverted pendulum. The double inverted pendulum consists of an inverted pendulum with a deliberately included flexible mode. With the two-loop control, the controller can be designed in two design steps.

First, H_∞ design is used to stabilize the pendulum. The design is focused on robustly stabilizing the pendulum with respect of the flexible mode frequency. A control scheme with a feedforward and a feedback controller and stable factor perturbations is applied to the pendulum. This has yielded a controller which could only guarantee stability for small flexible mode frequency perturbations.

The next step is to identify the stabilized pendulum and obtaining an accurate model of the pendulum. With this accurate model a new controller is designed with the H_∞ design procedure. Due to the bad model estimation and the used controller design, the two-loop design will not converge to an optimal controller.

M.Sc. Thesis, Measurement and Control Section (ER), Faculty of Electrical Engineering, Eindhoven University of Technology, The Netherlands, December 1994.

Contents

1 Introduction **7**
- 1.1 Flexible structures 7
- 1.2 Two-loop control 8
- 1.3 Problem definition 10

2 Derivation of the flexible inverted pendulum model **12**
- 2.1 Introduction 12
- 2.2 The nonlinear model 13
- 2.3 The linear model 16

3 Robust control **20**
- 3.1 Introduction 20
- 3.2 The standard problem 20
- 3.3 Structuring the inverted pendulum 21
- 3.4 Uncertainty modelling 25
- 3.5 Plant perturbations 26

4 Initial controller design **29**
- 4.1 Introduction 29
- 4.2 Classical first loop controller design 29
- 4.3 H_∞ robust design procedure 30
- 4.4 Simulation results 34

5 Identification **38**
- 5.1 Introduction 38
- 5.2 Preliminaries 38
- 5.3 The identification method 40
- 5.4 Model validation. 41

6 Second loop controller **46**
- 6.1 Introduction 46
- 6.2 Robust design procedure 46
- 6.3 Updating mechanism 49
- 6.4 Simulation results 51

7 Conclusions and recommendations **54**

A List of symbols **57**

B The simulink nonlinear model **60**

Chapter 1

Introduction

1.1 Flexible structures

Consider a system with an actuator, a mechanical beam and a sensor like in figure 1.1. One can recognize this construction in many mechanical servo systems like an arm in a CD player, the driving gear of a nozzle of a printer but also the dynamics of rockets etc. If the beam is excited, it will vibrate at its eigenfrequencies. These frequencies are called the flexible modes of the beam.

The position of the sensor is very important in the design of a servo controller of the beam. If the sensor is collocated with the actuator, the stability of this system can be guaranteed rather easily. However, if the sensor is moved along the beam, the flexible modes of the beam will become more important in the stability analysis [4]. In general, the stability of the beam is guaranteed by choosing a low bandwidth, which is far below the lowest flexible mode of the beam.

The question arises if it is possible to increase the bandwidth of the controlled beam across the lowest flexible mode. For this, an accurate model of the controlled beam is required. If no accurate model of the beam is available, we could obtain such a model with an identification procedure.

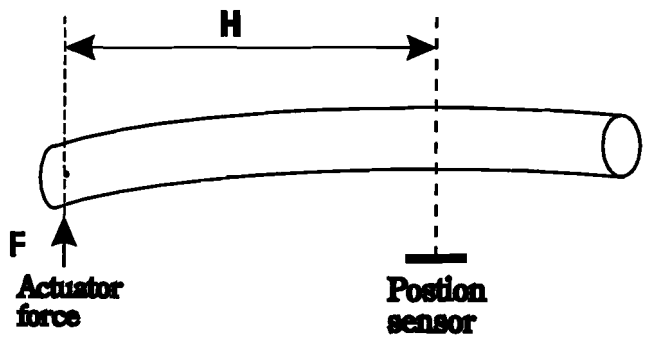

Figure 1.1: *Actuator, beam and sensor configuration.*

The flexible beam has theoretically an infinite number of flexible modes. If we want to

obtain a linear model of the beam, we have to approximate the nonlinear spatial model. We can only take a finite number of flexible modes into account. In [11] the effects of such an approximation is shown. The most important effect is the position of the system zeros. If an extra flexible mode is added to the linear model, an extra pole pair near the imaginary axis is appearing at the matching frequency of the flexible mode. However, the placement of all zeros of the model will change significantly. This is also the case for the zeros in the low frequency range of the model. Even zero pairs can swap from the imaginary axis to the real axis and vica versa. From this we conclude that beforehand the positions of the zeros are very uncertain.

To avoid problems described above, we will not only use an approximated model, but also an approximated experimental system. This is a 1st order approximation of a flexible beam and is described in chapter 2. In this way we can concentrate on stabilizing and optimizing this particular flexible beam. In a sequential stage, we can try to apply these results to a real flexible beam.

1.2 Two-loop control

There are many control design procedures which are based on a linear model. For an accurate model it is often necessary to run an identification procedure on the plant involved. However, it is sometimes not possible to run such experiment. This is for example because of economical reasons or because the plant is unstable. Here it can be advantageous to use a two-loop control scheme.

Figure 1.2 shows the principle of the two loop control. Because the plant P_0 can or may not be identified in an open loop structure, an initial feedback controller C takes care of the stabilization or quality control of the output. The plant P_0 and the feedback controller C are now treated as a new plant P_C,

$$P_C = \frac{P_0}{1 + CP_0}, \quad P_0 = \frac{P_C}{1 - P_C C}. \tag{1.1}$$

Zhu [15] showed that if the dynamics of the fed back system are known, it is possible to design a new controller which can optimize the plant's performance. First the fed back system is identified. Then a new controller ΔC is designed, which optimizes the fed back system. The two controllers C and ΔC are combined to a new controller C. Now we can repeat the procedure described above until the controller C will converge to a final controller.

After some time, the dynamics of the plant can change. If the procedure is repeated we find a new controller adapted to the new dynamics of the system. In this way we get an adaptive controller.

The two loop control structure has even some advantages over other schemes:

- When the available model of the system gets more accurate, better control can be achieved with the second loop controller.

- If the first loop controller is implemented, the identified system model P_C will be more accurate because the new controller will improve the effect of linearization, stationarization, effective order reduction and transient time reduction even more.

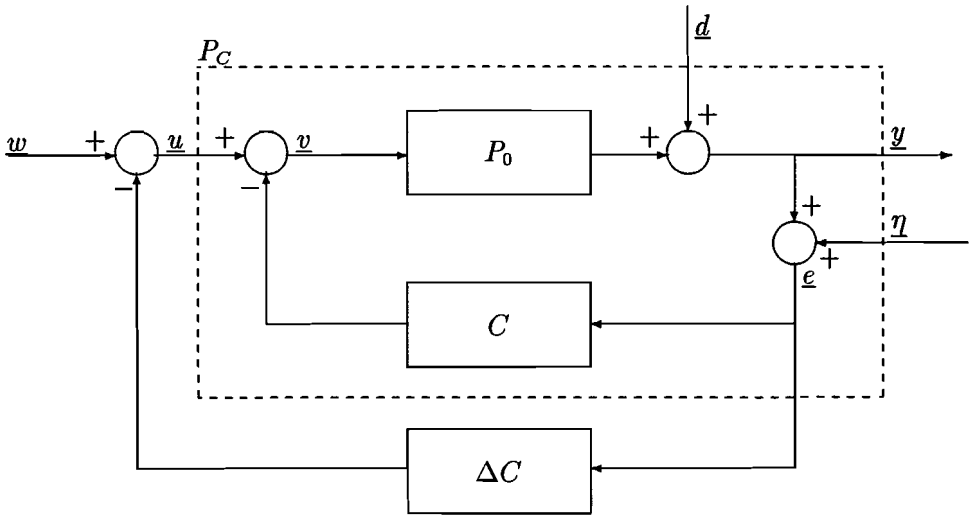

Figure 1.2: *Principle of two loop control.*

According to Zhu [15] the variances of the estimated system model $\hat{P}_C$ is proportional to the square of the sensitivity of the system. So if we achieve a low sensitivity in the band of interest, it will result in an accurate model.

$$var[\hat{P}_C(e^{(j\omega)}] \approx \frac{n}{N}\frac{\Phi_d}{\Phi_u} \mid S|^2 \tag{1.2}$$

With:

$\hat{P}_C$	:	Estimated closed loop system.
Φ_d, Φ_u	:	Power spectral density of d and u respectively.
n	:	Model order.
N	:	Number of samples.
S	:	The real sensitivity: $S = (I + P_0C)^{-1}$.

Thus far, we have put no constraints on the initial controller. Vidyasagar [13] showed that the first loop controller puts no constraints on the effect of the second loop controller if the process is strongly stabilizable. Strongly stabilizable means that the number of all real poles between two zeros in the Right Half Plane (RHP) is even (including zeros at infinity). In this way, it is allways possible to draw all unstable poles to the Left Half Plane with a stable controller.

More generally, a controller can consist of both a feedforward and a feedback controller. This configuration is shown in figure 1.3. In this figure, the updating of the controller is also generalized. It now consist of an identification block, a controller design block and a controller update block.

If a new controller is designed, we get the structure of figure 1.4. The plant P_0 is provided with a new feedback controller ΔC_{fb} and a new feedforward controller ΔC_{ff}. The former feedforward controller C_{ff} will be replaced by ΔC_{ff} and the feedback controllers are added.

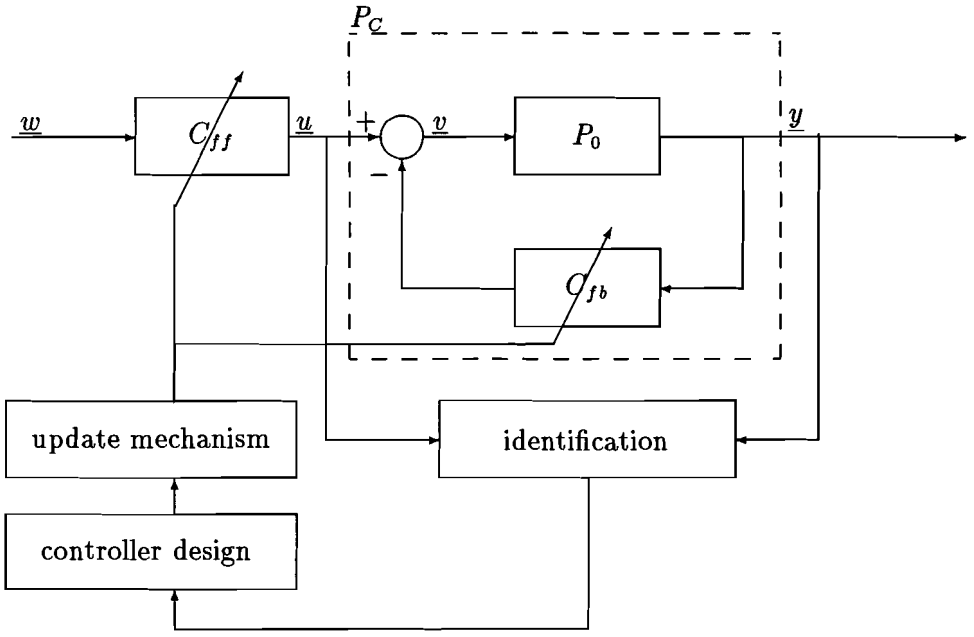

Figure 1.3: *General two loop adaptive control scheme.*

A straightforward adding of transfer functions will blow up the order of both controllers. The order of the controllers will grow without bound. To limit the order of the controllers, we have to use an order reduction method. This order reduction is the main function of the controller updating block.

1.3 Problem definition

A flexible Inverted Pendulum (IP) as described in chapter 2 is an application which concerns both the flexible structure problem and the two-loop control. Because the IP is unstable, it is difficult to identify this system. This can be solved by using an initial robust controller and applying the two-loop structure. The IP is an approximation of a real flexible beam. We hope, however, to get some insight in the problems concerning such a beam.

Chapter 2 concerns with the modelling of the flexible Inverted Pendulum system P_0 based on physical parameters. In chapter 4 an initial stabilizing controller C is designed. Both a classical and a H_∞ robust design method are considered. For a better understanding of the H_∞ robust design method applied, chapter 3 introduces this method. Chapter 5 describes the identification procedure and chapter 6 the second loop controller design. In chapter 7 some conclusions and recommendations are connected with these results.

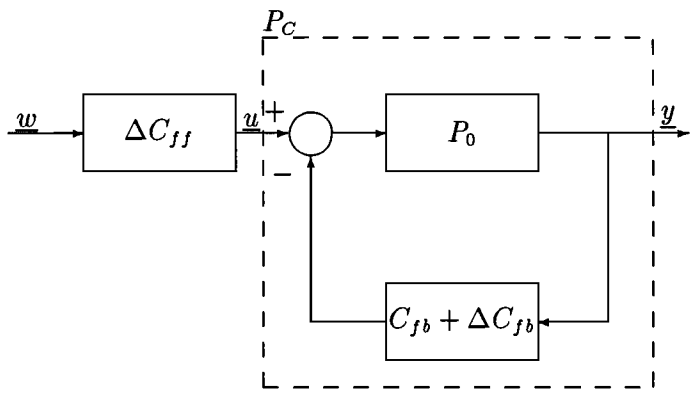

Figure 1.4: *Updating the feedforward and the feedback controller.*

Chapter 2

Derivation of the flexible inverted pendulum model

2.1 Introduction

This chapter deals with the structural modelling of the inverted pendulum (IP). After this introduction, a nonlinear model is derived. This model will be used for simulation purposes. This model is then linearized and discretized, so that it can be used as a basis for designing the first loop controller. Like figure 2.1 shows, the IP consists of 2 rods, which are connected at each other with a spring. This is mounted on the arm of a xy-recorder in such a way that the flexible rod can move in one plane only. Finally, a feedback signal must be available for controlling the IP. Therefore, the position of the second rod at height H is measured with a position sensor.

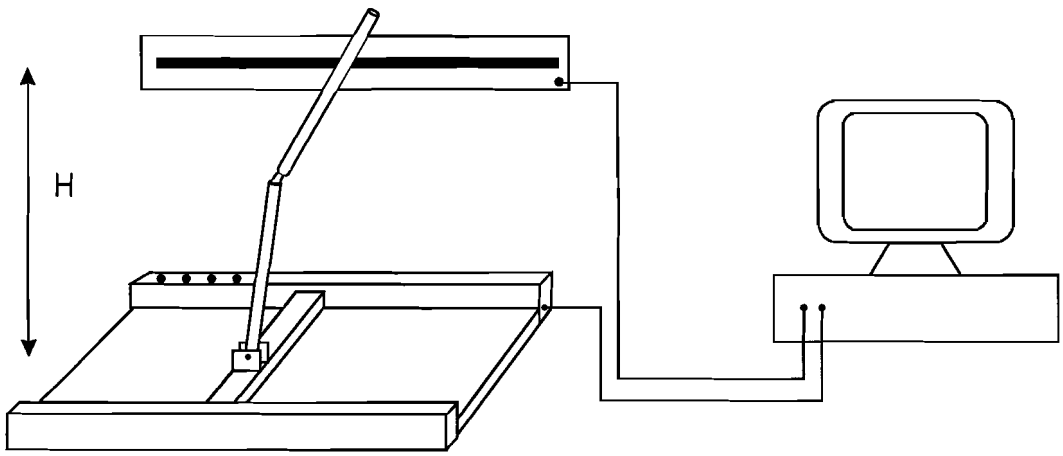

Figure 2.1: *Experimental system.*

The nonlinear model will be used to simulate the IP. In this way, the various designed controllers can be tested. The nonlinear model will also be used for the derivation of the linear model.

The linear structural model will be used to design a nonoptimal robust controller. The only purpose of this controller is to stabilize the IP.

Because both structural models will not be used to design an optimal controller, therefore a identification procedure is used, a number of approximations are introduced in the nonlinear model.

- The model contains only linear dynamical components. The nonlinearity of the IP will be caused only by the kinematical properties of the IP. Actually the various body's of the IP system are moving in various coördinate systems. There is a certain relationship between these systems dependent on the angles φ_1 and φ_2. These relationships are nonlinear. Further, the kinematical properties of the IP can also introduce nonlinear centrifugal and coriolis forces.

- The internal behavior of the xy-recorder is unknown. Only the linear behaviour from the input voltage to the position of the arm is available. However, the IP will apply a force to the xy-recorder's arm but it is not possible to use this force as an input signal of the xy-recorder. A solution for this problem is simply to neglect this feedback force, which is altogether very small.

- The dynamical model of the xy-recorder. We assume that the xy-recorder is a second order process, with the undamped frequency ω_r and the damping ratio β_r as the characteristic parameters.

2.2 The nonlinear model

Because there is no feedback from the IP to the xy-recorder, we can separate these systems and start with the IP. An important part of this derivation can also be found in [9]. The starting-point is the model in figure 2.2. Note that an extra mass is added to the system, which represents the cart on which the IP is mounted. The reason for this extra mass is that later on we will use Lagrange's equation of motion. Essentially this is a set of equations, which balances forces or torques on a mass. However, our system has as input signal the reference position of the xy-recorder's arm. This signal will be introduced naturally.

The model in picture 2.2 has the following physical parameters:

m_i	:Mass of the i'th pendulum.	$[kg]$
l_i	:Length between the i'th axis and the center of gravity.	$[m]$
J_i	:Moment of inertia about the center of gravity.	$[kgm^2]$
c_i	:Friction constant.	$[Nms]$
M	:Mass of the cart.	$[kg]$
L	:Length of the first pendulum.	$[m]$
F	:Friction constant between the cart and the monorail.	$[Nm^{-1}s]$
g	:Acceleration of gravity.	$[ms^{-2}]$
K	:Spring constant	$[Nm]$
U_0	:Rest energy spring	$[Nm]$

And f is a force applied to the mass of the cart. This system has the following kinetic (T), potential (U) and loss (D) energy:

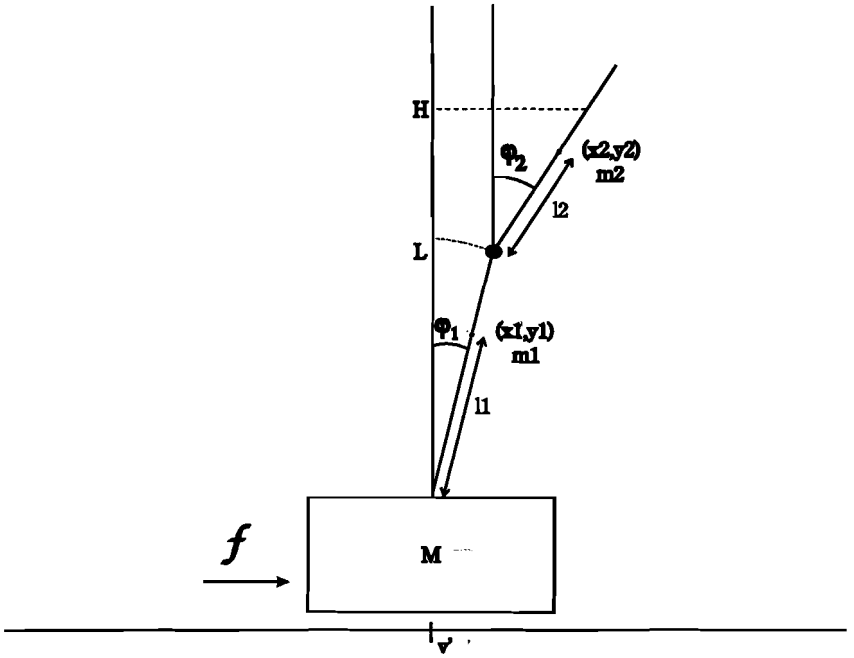

Figure 2.2: *Approximated model of the inverse pendulum with a flexible mode.*

$$T = \frac{1}{2}m_1(\dot{x}_1^2 + \dot{y}_1^2) + \frac{1}{2}m_2(\dot{x}_2^2 + \dot{y}_2^2) + \frac{1}{2}J_1\dot{\varphi}_1^2 + \frac{1}{2}J_2\dot{\varphi}_2^2 + \frac{1}{2}M\dot{v}'^2, \tag{2.1}$$

$$U = (m_1 l_1 + m_2 L)g\cos\varphi_1 + m_2 l_2 g\cos\varphi_2 + \frac{1}{2}K(\varphi_2 - \varphi_1)^2 + U_0, \tag{2.2}$$

$$D = \frac{1}{2}c_1\dot{\varphi}_1^2 + \frac{1}{2}c_2(\dot{\varphi}_2 - \dot{\varphi}_1)^2 + \frac{1}{2}F\dot{v}'^2. \tag{2.3}$$

The variables x_1, x_2, y_1, y_2 are dependent of the variables v', φ_1, φ_2

$$x_1 = v' + l_1\sin\varphi_1, \quad x_2 = v' + L\sin\varphi_1 + l_2\sin\varphi_2,$$
$$y_1 = l_1\cos\varphi_1, \quad y_2 = L\cos\varphi_1 + l_2\cos\varphi_2.$$

The expressions for the various kinds of energies are substituted in Lagrange's equation of motion:

$$\frac{d}{dt}\frac{\partial T}{\partial \dot{\underline{x}}_l} - \frac{\partial T}{\partial \underline{x}_l} + \frac{\partial U}{\partial \underline{x}_l} + \frac{\partial D}{\partial \dot{\underline{x}}_l} = \underline{f}_l. \tag{2.4}$$

Here $\underline{x}_l = [v', \varphi_1, \varphi_2]^t$ is a state vector containing all independent variables and $\underline{f}_l = [f, 0, 0]^t$ is an exogene force/torque vector applied on the rigid bodies of the system.

The substitution of 2.1, 2.2 and 2.3 in 2.4 yields

$$\begin{aligned} f &= (m_1+m_2+M)\ddot{v}' + (m_1l_1+m_2L)\cos(\varphi_1)\ddot{\varphi}_1 + m_2l_2\cos(\varphi_2)\ddot{\varphi}_2 - \\ &\quad -m_2l_2\sin(\varphi_2)\dot{\varphi}_2^2 + F\dot{v}', \end{aligned} \tag{2.5}$$

$$\begin{aligned} 0 &= (m_1l_1+m_2L)\cos(\varphi_1)\ddot{v}' + (m_1l_1^2+m_2L^2+J_1)\ddot{\varphi}_1 + \\ &\quad +m_2Ll_2\cos(\varphi_1-\varphi_2)\ddot{\varphi}_2 + m_2Ll_2\sin(\varphi_1-\varphi_2)\dot{\varphi}_2^2 - \\ &\quad -(m_1l_1+m_2L)g\sin(\varphi_1) - K(\varphi_2-\varphi_1) + (c_1+c_2)\dot{\varphi}_1 - c_2\dot{\varphi}_1, \end{aligned} \tag{2.6}$$

$$\begin{aligned} 0 &= m_2l_2cos(\varphi_2)\ddot{v}' + m_2l_2L\cos(\varphi_1-\varphi_2)\ddot{\varphi}_1 + (m_2l_2^2+J_2)\ddot{\varphi}_2 - \\ &\quad -m_2l_2L\sin(\varphi_1-\varphi_2)\dot{\varphi}_1^2 - gm_2l_2\sin(\varphi_2) - K(\varphi_1-\varphi_2) - \\ &\quad -c_2(\dot{\varphi}_1-\dot{\varphi}_2). \end{aligned} \tag{2.7}$$

These equations are force and torque balances on the cart, the first rod and the second rod respectively. Because there is no structural information available about the xy-recorder, it is not possible to implement equation 2.5. As stated earlier we know only the transfer function from input voltage v to the position of the arm of the xy-recorder v'. This is a general equation of a linear second order process:

$$\ddot{v}' = -2\beta_r\omega_r\dot{v}' - \omega_r^2v' + \omega_r^2v. \tag{2.8}$$

The only exogene signal in equations 2.6 and 2.7 is $\ddot{v}'$. This signal can be derived with equation 2.8. In this way equation 2.5 can be replaced by equation 2.8. It is now possible to place the equations 2.6, 2.7 and 2.8 in a state space setting. A general nonlinear state space equation is:

$$\begin{aligned} E(\underline{x})\dot{\underline{x}} &= \underline{f}(\underline{x}) + \underline{g}(\underline{x})v \\ \underline{y} &= \underline{h}(\underline{x}) \end{aligned} \tag{2.9}$$

The state vector is defined as:

$$\underline{x} = \begin{bmatrix} v' & \varphi_1 & \varphi_2 & \dot{v}' & \dot{\varphi}_1 & \dot{\varphi}_2 \end{bmatrix}^t. \tag{2.10}$$

Define:

$$E(\underline{x}) = \begin{bmatrix} I & 0 \\ 0 & E_{22} \end{bmatrix}, \tag{2.11}$$

$$E_{22} = \begin{bmatrix} 1 & 0 & 0 \\ (m_1l_1+m_2L)\cos\varphi_1 & m_1l_1^2+m_2L^2+J_1 & m_2l_2L\cos(\varphi_1-\varphi_2) \\ m_2l_2\cos\varphi_2 & m_2l_2L\cos(\varphi_1-\varphi_2) & m_2l_2^2+J_2 \end{bmatrix}, \tag{2.12}$$

$$\underline{f}(\underline{x}) = \begin{bmatrix} \dot{v}' \\ \dot{\varphi}_1 \\ \dot{\varphi}_2 \\ -2\beta\omega_0\dot{v}' - \omega_0^2v' \\ -m_2l_2L\sin(\varphi_1-\varphi_2)\dot{\varphi}_2^2 + (m_1l_1+m_2L)g\sin\varphi_1 + ... \\ +K(\varphi_2-\varphi_1) - c_1\dot{\varphi}_1 + c_2(\dot{\varphi}_2-\dot{\varphi}_1) \\ +m_2l_2L\sin(\varphi_1-\varphi_2)\dot{\varphi}_2^2 + m_2l_2g\sin\varphi_2 - K(\varphi_2-\varphi_1) - c_2(\dot{\varphi}_2-\dot{\varphi}_1) \end{bmatrix} \tag{2.13}$$

$$\underline{g}(\underline{x}) = \begin{bmatrix} 0 & 0 & 0 & \omega_0^2 & 0 & 0 \end{bmatrix}^t, \tag{2.14}$$

$$\underline{h}(\underline{x}) = [v' + L\sin\varphi_1 + (H - L\cos\varphi_1)\sin\varphi_2]. \tag{2.15}$$

This can be found straightforward with equations 2.6, 2.7 and 2.8. This nonlinear model is implemented in SIMULINK for simulation purpose. The SIMULINK implementation can be found in appendix B. For implementation, the matrix $E(\underline{x})$ has to be inverted. To simplify this, we used a-priori knowledge of the physical system. We know beforehand that the xy-recorder is separated from the IP. So we can cascade these two systems. In this case, the dimension of the vectors and matrices are reduced with 2. The upper parts of the system vectors are not needed in the implementation. The lower parts of the system vectors determine $\ddot{\varphi}_1$ and $\ddot{\varphi}_2$. From these signals we can derive the states by means of integration. In this way we only have to invert a 2x2 matrix.

2.3 The linear model

The starting-point of the linear model is the nonlinear model. For a linearization around $a = 0$ we use the following approximations:

$$\begin{aligned} \sin(a) &= a, \\ \cos(a) &= 1, \\ a^2 &= 0. \end{aligned}$$

Where a stands for φ_1, φ_2, $\dot{\varphi}_1$ and $\dot{\varphi}_2$. This yields the linear state space system

$$\begin{aligned} E\dot{\underline{x}} &= A\underline{x} + Bv \\ y &= C\underline{x} + Dv \end{aligned}, \tag{2.16}$$

and the matrices are defined as:

$$E = \begin{bmatrix} I & 0 \\ 0 & E_{22} \end{bmatrix}, \tag{2.17}$$

$$E_{22} = \begin{bmatrix} 1 & 0 & 0 \\ m_1 l_1 + m_2 L & m_1 l_1^2 + m_2 L^2 + J_1 & m_2 l_2 L \\ m_2 l_2 & m_2 l_2 L & m_2 l_2^2 + J_2 \end{bmatrix}, \tag{2.18}$$

$$A = \begin{bmatrix} 0 & I \\ A_{21} & A_{22} \end{bmatrix}, \tag{2.19}$$

$$A_{21} = \begin{bmatrix} -\omega_0^2 & 0 & 0 \\ 0 & (m_1 l_1 + m_2 L)g - K & K \\ 0 & K & -K + m_2 l_2 g \end{bmatrix}, \tag{2.20}$$

$$A_{22} = \begin{bmatrix} -2\beta\omega_0 & 0 & 0 \\ 0 & -c_1 - c_2 & c_2 \\ 0 & c_2 & -c_2 \end{bmatrix}, \tag{2.21}$$

$$B = \begin{bmatrix} 0 & 0 & 0 & \omega_0^2 & 0 & 0 \end{bmatrix}^t, \tag{2.22}$$

$$C = \begin{bmatrix} 1 & L & H - L & 0 & 0 & 0 \end{bmatrix}, \tag{2.23}$$

$$D = 0. \tag{2.24}$$

Because the matrix E has to be inverted to find an explicit model, a comprehensive relation between the physical parameters and the IP is lost. In figure 2.3 the influence of some physical parameters on the dynamical behaviour is shown.

These physical variables are respectively the spring constant, the sensor height, the axis height (the total length remains constant) and the total length of the pendulum. The 'b' and 'e' indicates the beginning and ending of the root locus as far as they are shown on the plots. The '1x' indicates a pole which is not moving. If the axis height is varied in the second plot, the total length remains constant. In the last plot, not only the total length is varied but also the masses of the rods are changing proportionally.

Especially the zeros in these plots are interesting. If, for example the sensor height is moved along the beam, we observe that a RHP zero pair becomes a LHP zero pair, and finally reaches the real axis. Here it seems a logical choice to place the sensor as high as possible.

If the sensor height is changed from $0m$ to $1.4m$, the zero pair near the imaginary axis remains approximately at the same frequency, but the damping of the zero becomes less. So the higher the sensor is placed, the more this frequency is damped.

Further, it can be observed that the root locus of the spring constant looks alike the root locus of the rod length. Only the direction of the locus is inverted. This can be explained that if the rod length is increased also the mass and inertia of the rod is increased. If the spring constant remains the same, the resonance frequency will be lowered. Apparently this has approximately the same effect as remaining the mass and inertia the same and lowering the spring constant.

The IP is a SISO sytem. So from the state space model we can obtain a transfer function. We denote this transfer function as $H_p(s) = Y(s)/U(s)$.

For controlling the IP, we will use a discrete-time controller. So the final linear model has to be discretized. An important parameter in the discretizing process is the sample frequency. The sample frequency has to be chosen such that all the relevant dynamics are not lost during the transformation. We will find this frequency with the help of the bode plot of $H_p(j\omega)$ in figure 2.4. We choose a 1% criterium: if the transfer of a frequency is less than 1%, we will neglect the dynamics. From figure 2.4 we notice that this frequency is $30/2\pi \approx 4.8Hz$. If we use Shannon's theorem and take a safety margin of at least a factor 2, we find a sample frequency of $20Hz$. A pole zero diagram of the discretized model can be found in figure 2.5.

In this plot we can assign some properties of the IP to the poles of the zero pole diagram. We recognize the 2 inverted pendulum poles at the real axis. Further, we can distinguish both a zero and pole pair near the unit circle. These represent the flexible mode of the IP caused by the deliberate inserted spring. Finally, we can also recognize the poles caused by the dynamics of the xy-recorder.

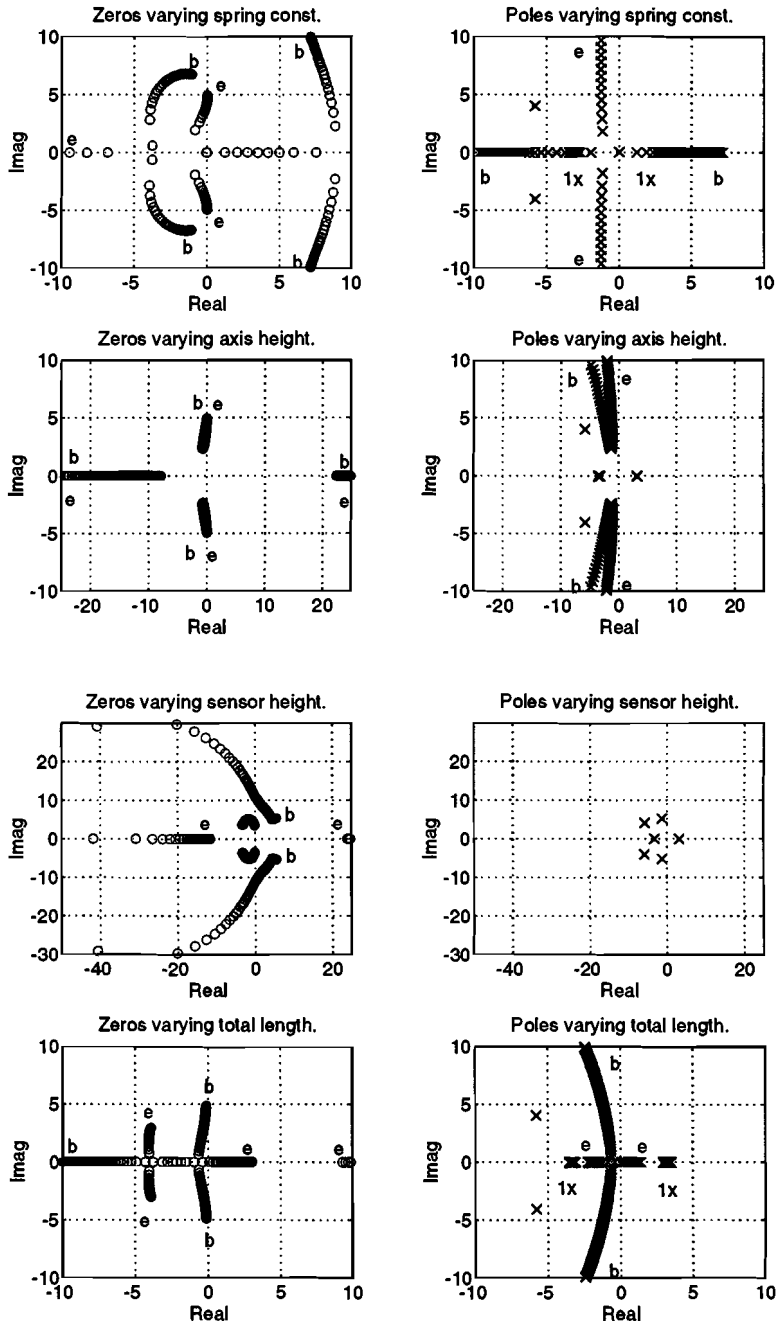

Figure 2.3: *Influence of some physical parameters on the dynamical IP behaviour.*

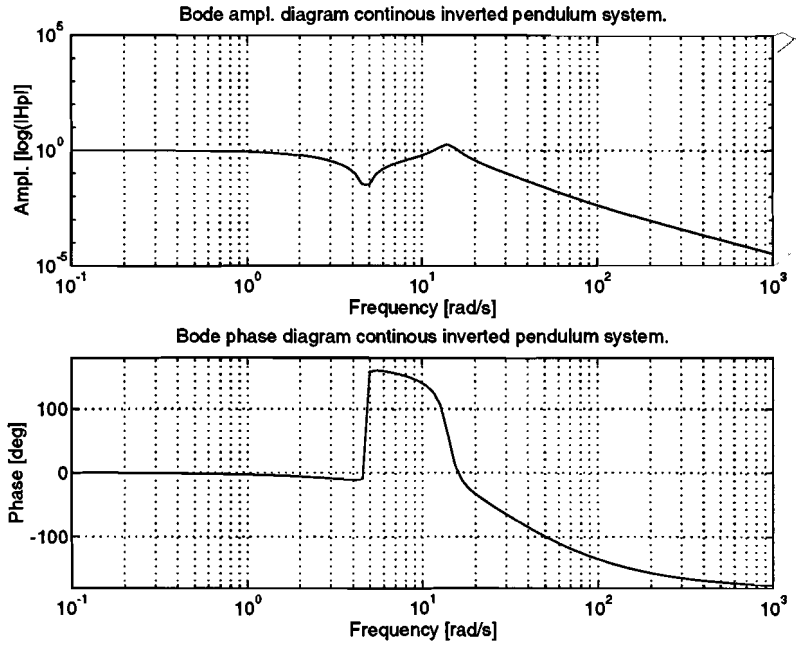

Figure 2.4: *Bode plot continous-time inverted pendulum model.*

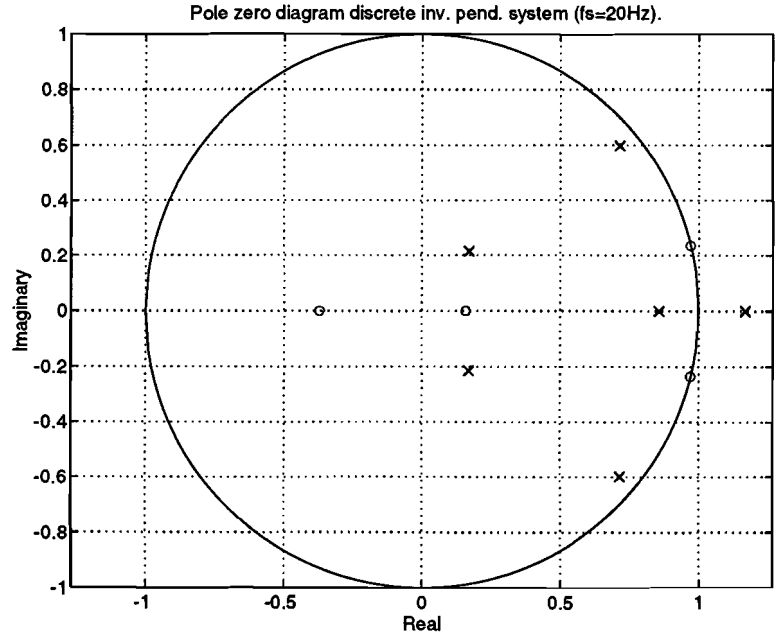

Figure 2.5: *Pole zero diagram of the discrete-time model.*

Chapter 3

Robust control

3.1 Introduction

As stated earlier, the main goal of the first loop controller is to stabilize the pendulum.

In chapter 4 a stabilizing controller will be designed with classical design tools. With the classical technique however, it is not possible to specify explicitly the robustness of the system. With an H_∞ approach, it is possible to specify both robustness and performance in the frequency domain.

In the second section of this chapter, the concept of the H_∞ design is presented. The main goal of this section is to give a background for the design procedure in the next sections. The 3rd section puts the inverted pendulum system in a H_∞ setting, while in the 4th section the stable factor perturbations are discussed. Finally in the 5th section the flexible mode perturbations are modelled.

3.2 The standard problem

The starting-point for the H_∞ design is depicted in figure 3.1. This is a general MIMO control structure. A number of exogene input signals $\underline{w}(t)$ are applied to the plant G. This plant has a number of measured output signals $\underline{y}(t)$. These output signals are fed back to the plant via a controller C. The control object for the controller C is to minimize the energy of the output signals $\underline{z}(t)$. All signals in figure 3.1 are assumed to be L_2 finite energy time functions. Note that in this chapter time functions and frequency functions are mixed. The time dependence is explicitly denoted but the frequency dependence is omitted for notational reasons.

The general plant G can be partitioned as:

$$\begin{bmatrix} \underline{z} \\ \underline{y} \end{bmatrix} = \begin{bmatrix} G_{11} & G_{12} \\ G_{21} & G_{22} \end{bmatrix} \begin{bmatrix} \underline{w} \\ \underline{u} \end{bmatrix}. \tag{3.1}$$

Minimizing the energy of $\underline{z}(t)$ is equivalent to minimizing α in:

$$\alpha := \inf_C \left[\sup_{w \in L_2} \frac{\|z\|_2}{\|w\|_2} \right] = \inf_C \|M_C\|_\infty \tag{3.2}$$

and M_C is defined as

$$\underline{z} = M_C \underline{w} = \left[G_{11} + G_{12} C \left(I - G_{22} C \right)^{-1} G_{21} \right] \underline{w}. \tag{3.3}$$

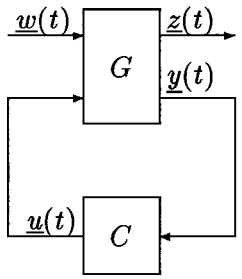

Figure 3.1: *The standard problem.*

The H_∞ norm of M_C is defined as

$$\|M_C\|_\infty = \sup_{\omega \in R} (\bar{\sigma}(M_C)). \tag{3.4}$$

Here $\bar{\sigma}(M_C)$ denotes the largest singular value of M_C. It is now possible to define the standard problem:

Standard problem: Find a real rational proper controller C to minimize the H_∞ norm of the transfer matrix M_C frow $\underline{w}$ to $\underline{z}$ under the constraint that C stabilizes G:

$$\alpha := \inf_C \|G_{11} + G_{12}C(I - G_{22}C)^{-1}G_{21}\|_\infty$$

The used solution of the standard problem is described by Glover [8]. The solution is based on putting the plant G in a state-space setting. Given a state-space characterization of all stabilizing controllers C_{st} such that

$$\|M_C(G, C_{st})\|_\infty < \gamma, \tag{3.5}$$

and γ is the H_∞-norm of the transfer matrix $M_C(G, C_{st})$. The optimal solution is then defined by: $\alpha := \min(\gamma)$.

3.3 Structuring the inverted pendulum

In this section, we put the pendulum in a H_∞ setting. The control scheme is depicted in figure 3.2. The scheme consist of the nominal process P_0, a feedforward and a feedback controller C_{ff} and C_{fb} and finally four loop shaping filters. Descriptions of these filters can be found in table 3.1. A structure with 2 controllers is chosen. With this extra degree of freedom, we enlarge the set of possible controllers which could result in a better robustness or performance.

The loop shape filters are augmented to the plant to put a constraint on the input and output signals. In this way it is possible to shape the input signals and weight the output signals in the frequency domain.

The configuration of figure 3.2 is now put in a standard problem setting of figure 3.3. This results in the following general plant:

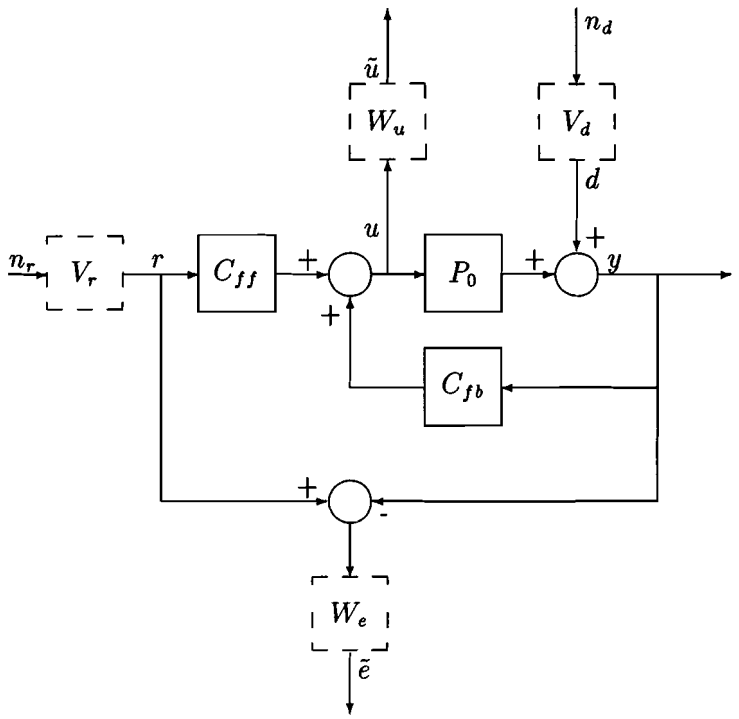

Figure 3.2: *Two-degree of freedom configuration.*

$$\underline{w} = \begin{pmatrix} n_d \\ n_r \end{pmatrix}, \tag{3.6}$$

$$\underline{z} = \begin{pmatrix} \tilde{e} \\ \tilde{u} \end{pmatrix}, \tag{3.7}$$

$$\begin{aligned} \|M_C\|_\infty &= \left\| \begin{array}{cc} M_{11} & M_{12} \\ M_{21} & M_{22} \end{array} \right\|_\infty \\ &= \left\| \begin{array}{cc} -W_e\,(I - P_0C_{fb})^{-1}\,V_d & W_e\left[I - (I - P_0C_{fb})^{-1}\,P_0C_{ff}\right]V_r \\ W_uC_{fb}\,(I - P_0C_{fb})^{-1}\,V_d & W_u\,(I - P_0C_{fb})^{-1}\,C_{ff}V_r \end{array} \right\|_\infty . \end{aligned} \tag{3.8}$$

For calculating the robust controller, the transfer functions of equation 3.8 have to be transformed to a state space model. This is described in [6]. Here also are discussed the conditions for the transfer functions and loop shaping filters.

The various transfer functions and weighting functions can be found in table 3.2. If the controller is designed such that $\gamma = 1$, the weighting and shaping filters put a direct constraint on the transfer functions of the controlled pendulum.

From table 3.2 the following relation between the transfer functions can be recognized:

$$M_{12}^* M_{21}^* - M_{11}^* M_{22}^* - M_{21}^* = M_{22}^* \tag{3.9}$$

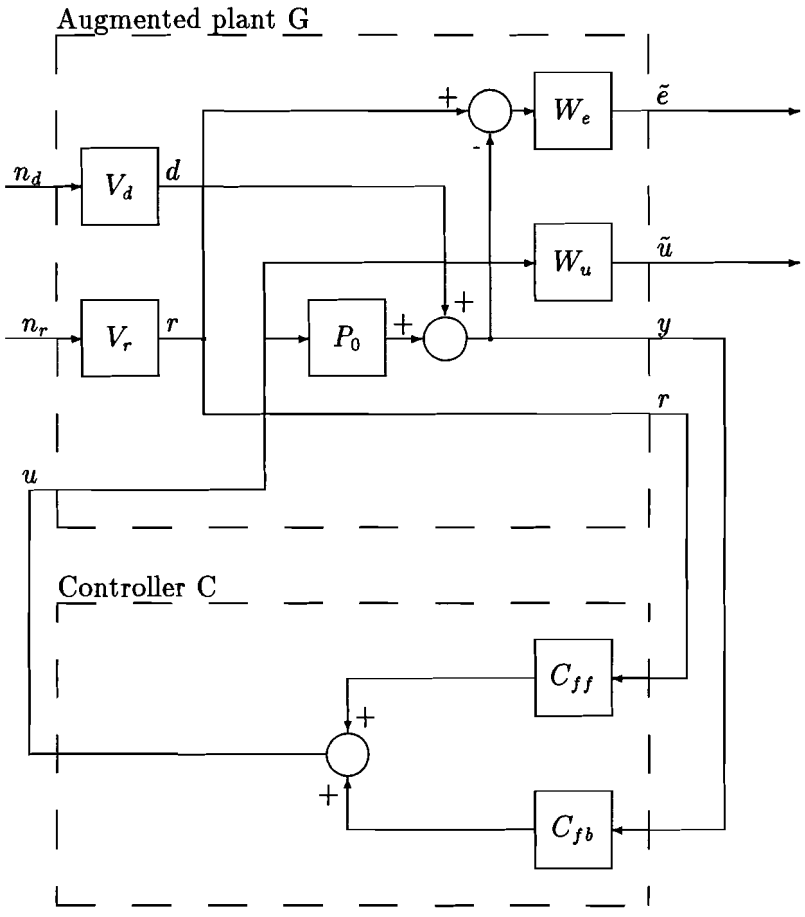

Figure 3.3: *Controlling scheme in general problem setting.*

Filter	Description
P_0	Nominal process model
V_d	Shaping model disturbances
V_r	Shaping reference signal
W_e	Weighting error signal
W_u	Weighting actuator signal
C_{fb}	Feedback controller
C_{ff}	Feedforward controller

Table 3.1: *SISO transfer functions of the augmented controlling scheme.*

Criterion	Description	Weighting function (scaled)	Transfer function
$M_{11} = \frac{\tilde{e}}{n_d}$	Disturbance reduction	$\frac{1}{\gamma} W_e V_d$	$M_{11}^* = -(I - P_0 C_{fb})^{-1}$
$M_{12} = \frac{\tilde{e}}{n_r}$	Signal tracking	$\frac{1}{\gamma} W_e V_r$	$M_{12}^* = I - (I - P_0 C_{fb})^{-1} P_0 C_{ff}$
$M_{21} = \frac{\tilde{u}}{n_d}$	Model robustness	$\frac{1}{\gamma} W_u V_d$	$M_{21}^* = C_{fb} (I - P_0 C_{fb})^{-1}$
$M_{22} = \frac{\tilde{u}}{n_r}$	Input saturation	$\frac{1}{\gamma} W_u V_r$	$M_{22}^* = (I - P_0 C_{fb})^{-1} C_{ff}$

Table 3.2: *Optimization critera of the robust design.*

Which can be verified by substitution. With this relation we try to put a extra constraint on the weighting and shaping filters. In this way we try to restrict the set of allowable filters, so designing these filters will become easier.

The upper and lower boundery for $|M_{22}^*|$ are:

$$|M_{22}^*| \leq |M_{12}^* M_{21}^*| + |M_{11}^* M_{22}| + |M_{21}^*| \tag{3.10}$$

$$|M_{22}^*| \geq ||\,|M_{12}^* M_{21}^*| - |M_{11}^* M_{22}^*|\,| - |M_{21}^*|| \tag{3.11}$$

The reciprocal scaled weighting functions are an upper bound for the transfer functions. In the design procedure one of the design aims is to minimize the distance between the transfer functions and their upper bounds. If this distance is zero, the transfer functions may be replaced by their upper bounds. In this way we find two sufficient conditions for the weighting filters:

$$\left|\frac{2\gamma}{W_e V_r V_d}\right| + \left|\frac{1}{V_d}\right| \geq \left|\frac{1}{V_r}\right| \quad \Rightarrow \quad |V_d| \leq |V_r| + \frac{2\gamma}{|W_e|}, \tag{3.12}$$

$$|M_{21}^*| \leq |M_{22}^*| \quad \Rightarrow \quad |V_d| \geq |V_r|. \tag{3.13}$$

Again these are no neccesary but sufficient conditions: They give an initial indication for the weighting filters and the 'optimal' weighting functions are likely to satisfy the conditions.

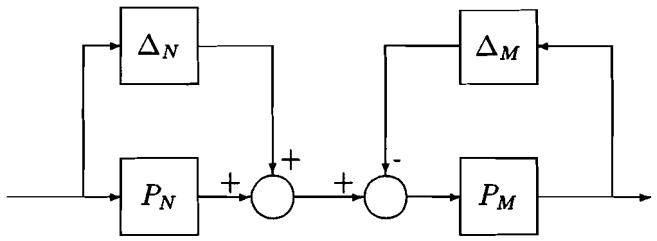

Figure 3.4: *Stable factor perturbation.*

3.4 Uncertainty modelling

For modelling the uncertainty of the plant, we have to introduce some model perturbations. For this purpose we will make use of the stable factor perturbation. If P_0 is the nominal plant and $\tilde{P}_0$ is the perturbed plant, we can divide this plant in a stable and unstable part,

$$P_0 = P_N P_M, \tag{3.14}$$

$$P_N = \frac{n_0}{d_N d_f}, \tag{3.15}$$

$$P_M = \frac{d_f}{d_M}. \tag{3.16}$$

where d_N are the stable poles and d_M the unstable poles of the model. Further d_f is a stable polynomial to make P_M proper. The model perturbations can now be defined as in figure 3.4. The perturbed model is expressed as

$$\left.\begin{array}{rcl} \tilde{P}_N &=& P_N + \Delta_N \\ \tilde{P}_M^{-1} &=& P_M^{-1} + \Delta_M \end{array}\right\} \Rightarrow \tilde{P}_0 = (P_N + \Delta_N)\left(P_M^{-1} + \Delta_M\right)^{-1}. \tag{3.17}$$

Now we can give a robustness constraint by considering the H_∞ bounds of the perturbations on the coprime factors P_N and P_M.

$$\|\Delta_M W_M^{-1}\ \Delta_N W_N^{-1}\|_\infty < \epsilon,\ W_N,\ W_N^{-1},\ W_M,\ W_M^{-1} \in RH_\infty. \tag{3.18}$$

A controller C will stabilize all perturbed plants $\tilde{P}_0$ if and only if:

$$\left\| \begin{array}{c} W_M (I - P_0 C)^{-1} P_M \\ W_N C (I - P_0 C)^{-1} P_M \end{array} \right\|_\infty \leq \epsilon^{-1}. \tag{3.19}$$

Optimization of the plant robustness with respect to stable factor perturbations is equal to:

$$\min_C \left\| \begin{array}{c} W_M (I - P_0 C)^{-1} P_M \\ W_N C (I - P_0 C)^{-1} P_M \end{array} \right\|_\infty. \tag{3.20}$$

This optimization criterium can be compared with the optimization criteria of table 3.2. If we now choose $V_d = P_M^{(mir)}$, $W_u = W_N$ and $W_e = W_M$ then the optimization of the plant

robustness with respect to stable factor perturbations is equal to the disturbance reduction and the model robustness criterion of table 3.2. $P_M^{(mir)}$ is P_M with all unstable parts mirrowed with respect of the imaginary axis. This is allowed because in equation 3.20 and equation 3.8 only the H_∞ norm is considered. The mirrowed poles are chosen because V_d should be stable and minimal phase. In this way, we lose some degrees of freedom by this choice of W_u and W_e, but solving the problem will become much easier.

The nominal and perturbed plant can be written as polynomials:

$$P_0 = \frac{n_0}{d_0} = \frac{n_0}{d_N d_M} = P_N P_M = \frac{n_0}{d_N d_f}\frac{d_f}{d_M}, \tag{3.21}$$

$$\begin{aligned} \tilde{P}_0 &= \frac{n_0 + \Delta_n}{d_0 + \Delta_d} = \tilde{P}_N \tilde{P}_M = (P_N + \Delta_N)\left(P_M^{-1} + \Delta_M\right)^{-1} \\ &= \left(\frac{n_0}{d_N d_f} + \Delta_N\right)\left(\frac{d_M}{d_f} + \Delta_M\right)^{-1}. \end{aligned} \tag{3.22}$$

This results in:

$$\Delta_N = \frac{\Delta_n}{d_N d_f}, \tag{3.23}$$

$$\Delta_M = \frac{\Delta_d}{d_N d_f}. \tag{3.24}$$

The derived descriptions of the uncertainties Δ_N and Δ_M can be used in the design of the weighting filters:

$$\|W_e^{-1}\Delta_M \; W_u^{-1}\Delta_N\|_\infty < \epsilon, \; V_d = P_M. \tag{3.25}$$

If a boundary for Δ_n and Δ_d is defined, we can find a lower boundery for the weighting filters:

$$|W_u| \geq \sup_{\Delta_n} \left|\frac{\Delta_n}{d_N d_f}\right|, \tag{3.26}$$

$$|W_e| \geq \sup_{\Delta_d} \left|\frac{\Delta_d}{d_N d_f}\right|. \tag{3.27}$$

In the next section we will derive an expression for Δ_n and Δ_d.

3.5 Plant perturbations

With the stability analysis, we will take only the perturbation of the pole pair and zero pair near the unit circle into account. These pairs are further on treated as ordinary second order sections with a undamped frequency and a relative damping as parameters. The disturbed parameters can than be written as a nominal part and a deviation part:

$$\begin{aligned} \tilde{\omega}_d &= \omega_d(1 + \Delta\omega_d), \\ \tilde{\beta}_d &= \beta_d(1 + \Delta\beta_d), \\ \tilde{\omega}_n &= \omega_n(1 + \Delta\omega_n), \\ \tilde{\beta}_n &= \beta_n(1 + \Delta\beta_n). \end{aligned} \tag{3.28}$$

The perturbed plant becomes

$$\tilde{P}_0 = \frac{\tilde{n_{nf}}\left(s^2 + 2\tilde{\beta}_n\tilde{\omega}_n s + \tilde{\omega}_n^2\right)}{d_{nf}\left(s^2 + 2\tilde{\beta}_d\tilde{\omega}_d s + \tilde{\omega}_d^2\right)}, \tag{3.29}$$

$$\tilde{n_{nf}} = n_{nf}\frac{(1+\Delta\omega_d)^2}{(1+\Delta\omega_n)^2}. \tag{3.30}$$

Here n_{nf} and d_{nf} are the not perturbed parts of the transfer function of the model, although a perturbed $\tilde{n_{nf}}$ is used. This is because the static gain of the pendulum is independent of the flexible mode. However, if we deviate the undamped frequency's in equation 3.30, the static gain will deviate also. To overcome this problem, the static gain is compensated. This becomes clear in equation 3.31

$$\tilde{P}_0 = \frac{n_{nf}}{d_{nf}}\frac{(1+\Delta\omega_d)^2}{(1+\Delta\omega_n)^2}\frac{\left[s^2 + 2\beta_n(1+\Delta\beta_n)\omega_n(1+\Delta\omega_n)s + \omega_n^2(1+\Delta\omega_n)^2\right]}{\left[s^2 + 2\beta_d(1+\Delta\beta_d)\omega_d(1+\Delta\omega_d)s + \omega_d^2(1+\Delta\omega_d)^2\right]}. \tag{3.31}$$

It is now possible to distinguish a nominal part and a perturbed part in both the numerator and denominator

$$\tilde{P}_0 = \frac{n_0 + \Delta_n}{d_0 + \Delta_d}, \tag{3.32}$$

$$\Delta_n = n_{nf}\left\{\left[\frac{1}{(1+\Delta\omega_n)^2} - 1\right]s^2 + 2\beta_n\omega_n\left[\frac{(1+\Delta\beta_n)(1+\Delta\omega_n)}{(1+\Delta\omega_n)^2} - 1\right]s\right\}, \tag{3.33}$$

$$\Delta_d = d_{nf}\left\{\left[\frac{1}{(1+\Delta\omega_d)^2} - 1\right]s^2 + 2\beta_d\omega_d\left[\frac{(1+\Delta\beta_d)(1+\Delta\omega_d)}{(1+\Delta\omega_d)^2} - 1\right]s\right\}. \tag{3.34}$$

Figure 3.5 shows $|\Delta_n|$ as function of the perturbations $\Delta\omega_n$ and $\Delta\beta_n$. This function is evaluated at the resonance frequency $s = j\omega_d$ of the flexible mode. The figure shows a convex function.

As long as $|\Delta\omega_n|$ and $|\Delta\omega_d|$ are smaller than 1 (100% deviation), $|\Delta_n|$ and $|\Delta_d|$ will be convex for all ω. This can be comprehended as follows: Both absolute values of the perturbed polynomial coefficients in equation 3.33 are convex and have the same minimum $(|\Delta\omega_n|, |\Delta\beta_n|) = (0,0)$. If 2 convex functions with the same minimum are weighted and added, also the new function will be convex with the same minimum.

For calculating the supremum of the weighting functions of equations 3.26 and 3.27, we will evaluate $|\Delta_n|$ at the 4 bounderies points $(\pm\Delta\omega_n, \pm\Delta\beta_n)$ and use the maximum of these values for calculating the supremum. For $|\Delta_d|$, the same argumentation can be used.

We have now presented the analytical tools with which H_∞ controllers will be designed in chapter 4 and chapter 6.

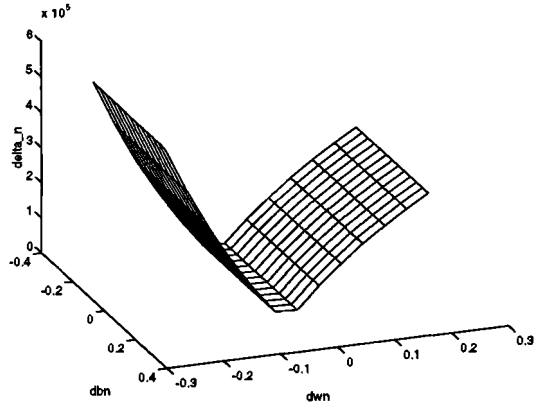

Figure 3.5: $|\Delta_n|$ *as function of* $\Delta\omega_n$ *and* $\Delta\beta_n$ *at* $s = j\omega_d$.

Chapter 4

Initial controller design

4.1 Introduction

There are 3 candidate design methods for the first loop controller: an LQR method, the classical design methods and a robust control design method.

The LQR method is based on the availability of the states of the IP. If these are not available, we can find them with an observer. So from a single output signal with an a-priori unknown noise signal, we have to extract 6 states. We expect the reliability of the states to be poor. Further, it is generally known that the LQR design method is only reliable if the states are reliable. This is in contrast with the classical methods with gain and phase margins and the robust design methods with explicit defined plant deviations. So in section 4.2 we will design the first loop controller with a classical method and the robust controller in section 4.3.

4.2 Classical first loop controller design

A classical controller can be designed in the s-domain, z-domain or ω domain. Because we have a discrete model that is already described in the z-domain and we will use a discrete controller, we will design the controller in the the z-domain.

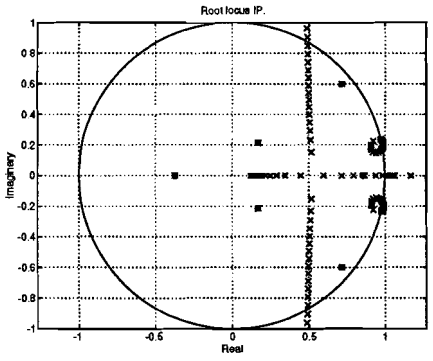

Figure 4.1: *Root locus controllor and system with pole zero cancellation.*

The design of the feedback controller C_{fb} is based on placing extra poles and zeros in the open loop transfer function. This will influence the root locus of the open loop system. With the help of this root locus we will choose the loop gain such that we can achieve our control goals.

For the first loop controller we have only one control goal: stabilizing the IP. The IP has 5 poles and 4 zeros inside and 1 pole and 1 zero outside the unit circle. For stabilizing the IP we choose for a pole zero cancellation approach. All poles and zeros inside the unit circle are compensated. If the poles or zeros are very close to the unit circle, exact compensation can be dangerous because it can lead very easily to instabilities. In that case, the compensation pole or zero will be put in the neighbourhood of the pole or zero. Then we try to draw the unstable pole inside the unit circle. Because we have to compensate more poles than zeros, the corresponding regulator will not be proper. To overcome this problem we add an extra pole in $z = 0$ (an extra time delay). The root locus of this compensated system is shown in figure 4.1. From this root locus we conclude that pole zero cancellation is enough to stabilize the IP.

Finally we have to choose the loop gain. If the gain is chosen to low or to high, the IP is unstable. We denote these gain boundaries a K_l and K_h. So there is a range of gains where the IP is stable.

In general, the robustness of a classical designed controller is improved, if the loop gain is lowered. We can apply this rule of thumb also in this case. If the flexible mode frequency deviates from it's nominal value, the lower gain boundary K_l remains almost the same, while the upper boundery K_h changes dramatically. For this reason, the loop gain is chosen 10% above the lower gain boundary.

Next, the feedforward controller C_{ff} is designed. With this controller it is possible to adjust the tracking error and the actuator saturation. The controller is chosen such that the steady state error is zero. This can be achieved by choosing C_{ff} as a constant gain. This gain is the reciprocal value of steady state gain of the fed back inverted pendulum.

4.3 H_∞ robust design procedure

In this section a first loop robust controller is designed. With H_∞-control, this designing is equivalent with designing the loop shaping filters W_e, W_u, V_d and V_r. In chapter 3 we have already found constraints for these filters:

$$|V_d| \leq |V_r| + \frac{2\gamma}{|W_e|}, \tag{4.1}$$

$$|V_d| \geq |V_r|, \tag{4.2}$$

$$V_d = \frac{d_f}{d_M^{(mir)}}, \tag{4.3}$$

$$|W_u| \geq \sup_{\Delta_n} \left| \frac{\Delta_n}{d_N d_f} \right|, \tag{4.4}$$

$$|W_e| \geq \sup_{\Delta_d} \left| \frac{\Delta_d}{d_N d_f} \right|, \tag{4.5}$$

with constraints 4.1 and 4.2 as sufficient conditions. As stated earlier, we will concentrate on the robustness properties of the controller. These are specified by the weighting filters for

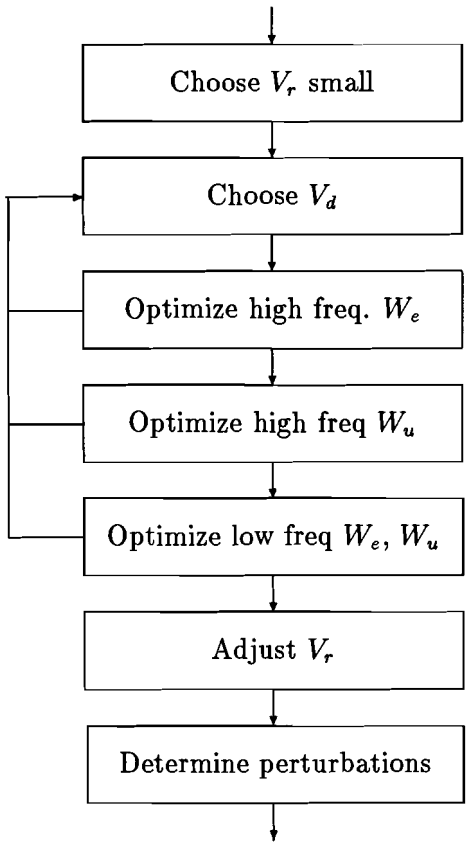

Figure 4.2: *Robustness optimization design procedure.*

the disturbance reduction $\frac{\gamma}{V_d W_e}$ and the model robustness $\frac{\gamma}{V_d W_u}$.

In general, the order of the controller is the sum of the order of the plant and the orders of the weighting and shaping filters. For this reason, we will choose the order of the filters as low as possible and start with 1st order filters.

As pointed out in Falkus [6] pp27, The weighting filters V_d, V_r and W_u have to be biproper. This is because the state space solution method puts constraints on the augmented plant G, which on their turn puts constraints on the weighting filters.

Because there is a clear relation between the weighting filter parameters and the magnitude frequency function of these filters, the filter design is performed in the continous-time. However, the controller will be designed in discrete-time. So the filters have to be transformed from the continous-time to the discrete-time. For the transformation algorithm, the bilinear transformation with frequency prewarping is used. This transformation maps the imaginary axis on the unit circle and only the frequency axis is deformated. To compensate this deformation a prewarping frequency can be entered. By means of frequency scaling beforehand, this frequency is not deformed during the transformation. We consequently used the resonance frequency as prewarping frequency, because this frequency is very sensitive for the deformation. A small frequency deviation at this frequency will cause a large magnitude deviation of the model.

Figure 4.3 shows the used design strategy. First, an initial V_r is designed. We will first try to optimize the robustness demand and next the performance demand. Because V_r has no influence on the robustness demands , the gain K_r is chosen small. In this way, both the tracking and the actuator saturation transfer functions are not the limiting weighting functions in the H_∞ norm. V_r is chosen lowpass, because this is conform to the applied input signal.

$$V_r^{(ini)} = \frac{K_r(s - z_r)}{(s - p_r)} = \frac{0.003(s + 0.5)}{(s + 0.005)}. \tag{4.6}$$

The next step is to define the disturbance weighting filter V_d.

$$V_d = \frac{d_f}{d_M^{(mir)}} = \frac{K_d(s - z_d)}{(s + 3.2)} = \frac{(s + 0.2)}{(s + 3.2)}. \tag{4.7}$$

Because d_M has an unstable pole and the weighting filters have to be stable RH_2, the pole is mirrowed with respect of the imaginary axis. This is allowed because only the magnitude of the weighting filters is considered in the H_∞ design.

The next parameter to be chosen is z_d. We will choose z_d smaller than the unstable pole, because this allows a higher robustness for higher frequencies. This is conform to the specified model perturbations, which show a relative large deviations for high frequencies (the resonance frequency).

The gain of the scaled weighting functions $\frac{\gamma}{V_d W_u}$ and $\frac{\gamma}{V_d W_e}$ is dependent on $\frac{\gamma}{K_d K_u}$ and $\frac{\gamma}{K_d K_e}$ respectively. During the design, K_u and K_e are used to change the gain of the scaled weighting functions. K_d is only used to avoid numerical problems and is set to the value 1.

Equation 4.4 and 4.5 implies that the disturbance reduction weighting function $\frac{\gamma}{V_d W_u}$ puts a constraint on the flexible mode pole (at 13.3 r/s) perturbation and the model robustness weighting function $\frac{\gamma}{V_d W_u}$ puts a constraint on the flexible mode zero (at 5 r/s) perturbation, Δ_d and Δ_n are dependent on these pole and zero perturbations respectively. The design of W_e and W_u is now divided in two steps. First we will perform a maximum effort to weight the disturbance reduction and model robustness at the pole and zero frequencies respectively. This is denoted as the high frequency optimization of W_e and W_u in figure 4.3.

The next step is to weight also the low frequency range of the transfer functions. This results in the following shaping filters:

$$W_e = \frac{0.5144(s + 3.1)}{(s + 0.2)}, \tag{4.8}$$

$$W_u = \frac{1.12(s + 0.1)}{(s + 40)}. \tag{4.9}$$

Then the performance demand will be satisfied, without changing the robustness of the system achieved thus far, the performance is increased by increasing the gain of V_r until γ will change. This results in the following input shaping filter:

$$V_r = \frac{0.2025(s + 0.5)}{(s + 0.005)}. \tag{4.10}$$

The shaping filters are shown in figure 4.3 and the various transfer functions are shown in figure 4.4.

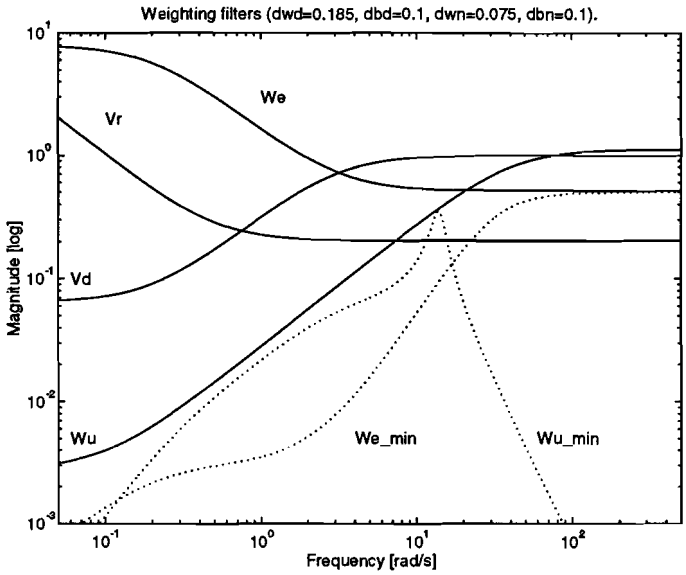

Figure 4.3: *Weighting filters:* $\Delta\beta_n = 10\%$, $\Delta\omega_n = 7.5\%$, $\Delta\omega_d = 18.5\%$, $\Delta\beta_d = 10\%$.

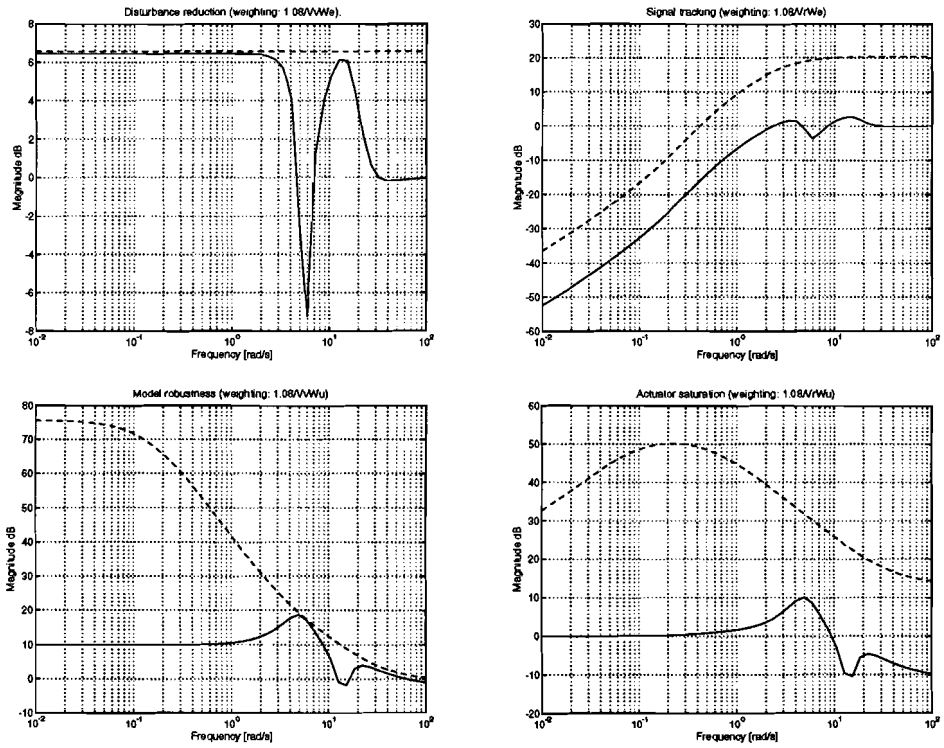

Figure 4.4: *Transfer functions with robust controller.*

With the obtained shaping functions W_e, W_u and V_d it is possible to derive the maximum allowable perturbation of the flexible mode pole and zero. This relation is derived via equations 4.3, 4.4, 4.5, 3.33 and 3.34.The design will only guarantee a stable pendulum, if the resonance frequency deviation is smaller than 18.5%.

The disturbance reduction (sensitivity) shows an amplification of $6dB$ of the noise. This is rather high.

Figure 4.4 shows that we have achieved a very good tracking. This implies that it is possible to find a more robust controller because in general a good tracking requires a small model perturbation.

4.4 Simulation results

In this section the robust and the classical designed first loop controller are compared.

The design procedure described in section 4.2 results in the feedforward controller C_{ff} and the feedback controller C_{fb}:

Classical 1st loop controller:

$$C_{ff} = -0.1014 \tag{4.11}$$

$$C_{fb} = \frac{-1.54z^5 + 4.03z^4 - 4.52z^3 + 2.49z^2 - 0.63z + 0.09}{z^5 - 1.63z^4 + 0.45z^3 + 0.30z^2 - 0.05z} \tag{4.12}$$

H_∞ robust 1st loop controller:

$$C_{ff} = 0.1\frac{-3.95z^7 + 5.85z^6 - 0.64z^5 - 4.97z^4 + 4.07z^3 - 1.12z^2 + 0.29z + 007}{z^7 - 2.05z^6 + 1.19z^5 + 0.37z^4 - 0.88z^3 + 0.58z^2 - 0.16z + 0.030} \tag{4.13}$$

$$C_{fb} = \frac{-1.07z^7 + 1.58z^6 - 0.17z^5 - 1.35z^4 + 1.10z^3 - 0.30z^2 + 0.08z + 0.0018}{z^7 - 2.05z^6 + 1.20z^5 + 0.37z^4 - 0.88z^3 + 0.58z^2 - 0.16z + 0.03} \tag{4.14}$$

To illustrate how the controller has stabilized the pendulum, the pole zero diagrams of the controllers are shown in figure 4.5 and figure 4.6.

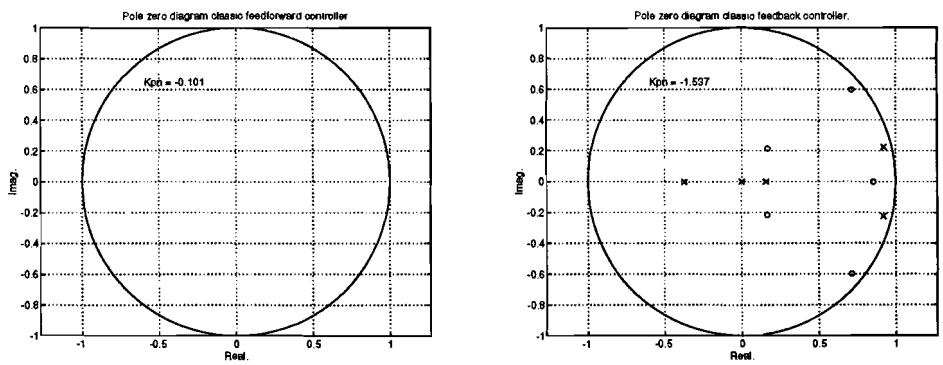

Figure 4.5: *Pole zero diagrams classical designed controller.*

To evaluate the robustness of the controlled pendulum, figure 4.7 and figure 4.8 show the stability area. These figures show for which values of absolute spring damping and spring

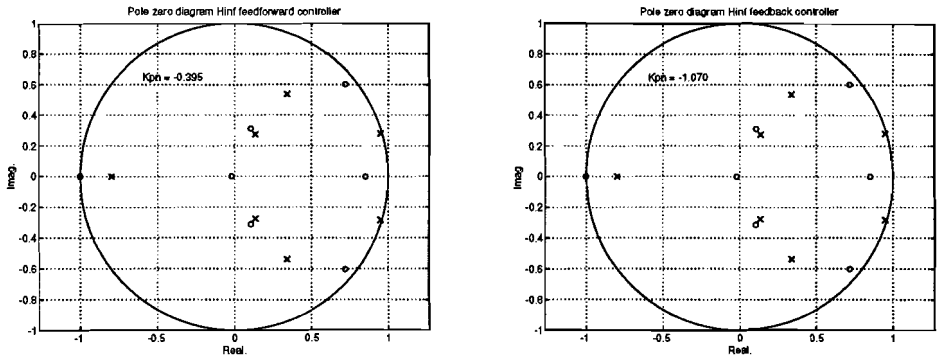

Figure 4.6: *Pole zero diagrams H_∞ designed controller.*

constants, the linear pendulum model remains stable. All other physical parameters are assumed to be exact. The 'x' denotes the nominal model.

The resonance frequency and the relative spring damping are strongly related to the spring constant and the absolute spring damping. Figure 4.7 shows that maximum allowable deviation of the resonance frequency before the pendulum becomes unstable is about 30% in the classical case and about 16% in the robust case. Based on these figures, the classical design is more robust than the H_∞ design.

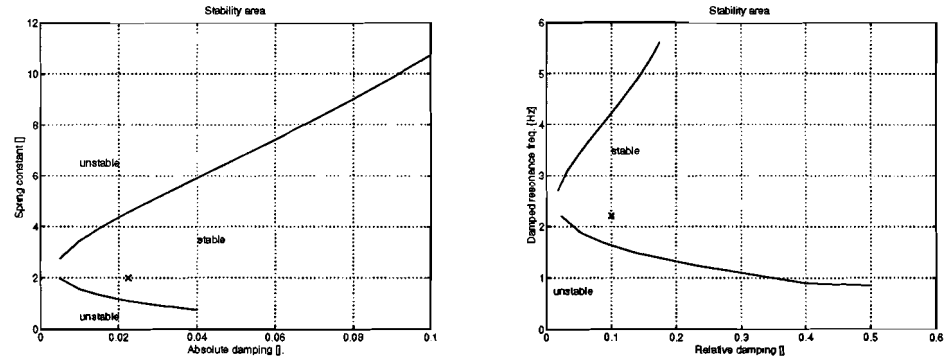

Figure 4.7: *Stability area classic controlled pendulum.*

Finally, the bode diagram of the controlled pendulum is compared for the two cases. Figure 4.10 shows the classical design and figure 4.11 the H_∞ design. The bandwidth of the pendulum of the classical design is quite low: $\frac{0.7}{2\pi} \approx 0.11Hz$. This is a direct consequence of chosing the loop gain as low as possible. The bode diagram of the H_∞ design shows a bandwidth of $\frac{3}{2\pi} \approx 0.48Hz$. It also can be noted, that the flexible mode frequency is not very strongly damped.

Another difference between the classical and the H_∞ design are the sensitivity functions (figure 4.9 and figure 4.4). For low frequencies the sensitivity of the classical design is about

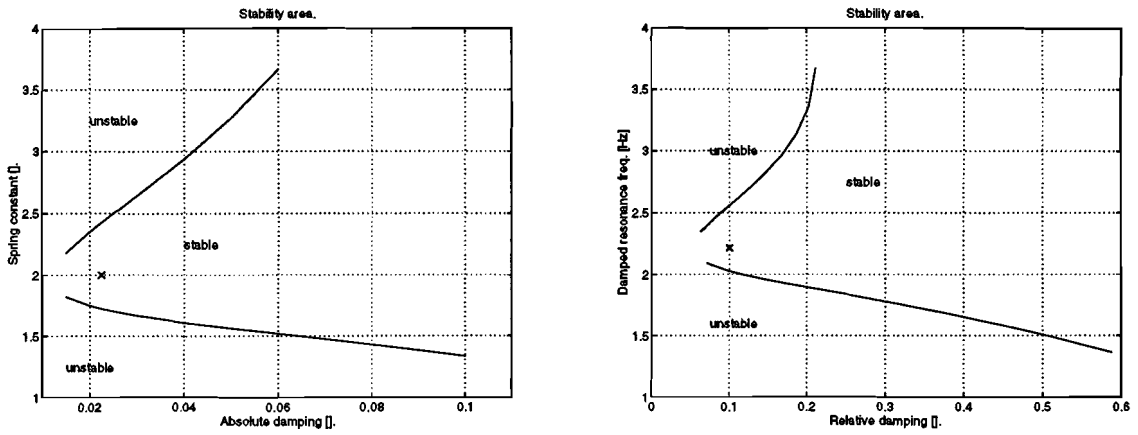

Figure 4.8: *Stability area H_∞ controlled pendulum.*

5 times larger than the sensitivity of the H_∞ design.

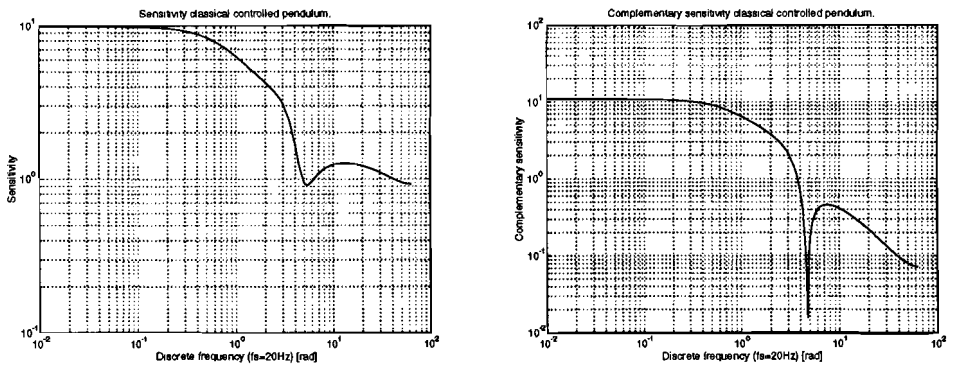

Figure 4.9: *Sensitivity and compl. sensitivity classical designed controller.*

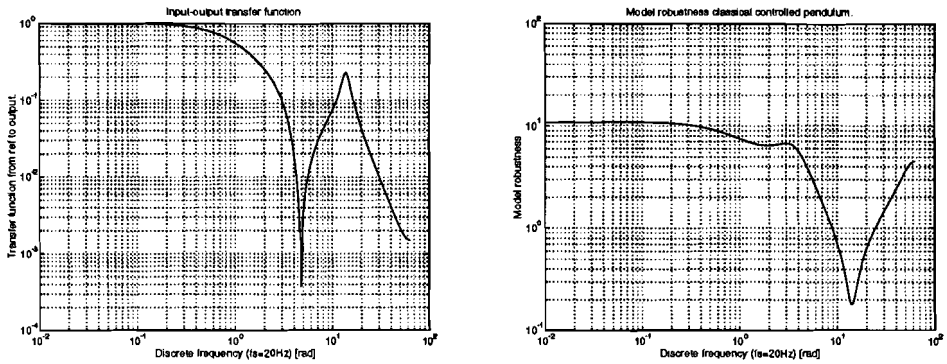

Figure 4.10: *Input-output transfer function and control sensitivity classical controlled pendulum.*

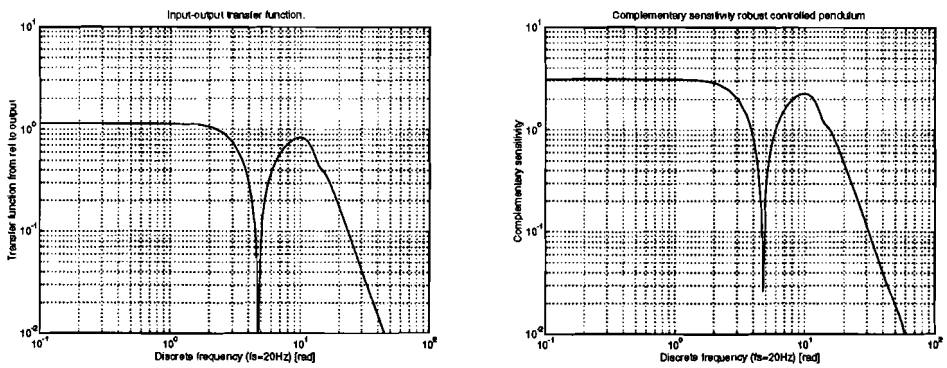

Figure 4.11: *Input-output transfer function and model robustness Hinf controlled pendulum.*

Chapter 5

Identification

5.1 Introduction

In this chapter, the inverted pendulum which is stabilized in chapter 4 will be identified. Our goal is to estimate an accurate black-box model, which can be used for the second loop controller. The identification is performed both with the classical and robust designed controller.The identification procedure can be separated in the following design steps

preliminaries and experiment Here the various experiment parameters are chosen such as the sample frequency, the experiment duration, model choice, input signal, noises.

model estimation Based on the collected data of the experiment, a structural model is estimated.

model validation The obtained model is validated and a decision is made whether or not to accept the model. If the model is not accepted, a new model can be estimated, or even the preliminaries could be changed.

5.2 Preliminaries

An important phase in the identification procedure is the preparation phase. In this phase the following considerations are taken:

model choice: At this moment, two different structural models are available: the linear model and the nonlinear model. We could ask ourselves if it is usefull to simulate with the nonlinear model. The nonlinear model contains three different types of nonlinearities.

To simulate the input saturation of the xy-recorder, its input is clipped.

The harmonical nonlinear relations are due to the relations of the different coordinate systems. The angles of these coordinate systems remain small ($< 15°$), which results in a reasonable accurate linearization.

There are centrifugal forces in the system. These cause small deviations with respect of the linear system.

Because of the centrifugal forces it is useful to simulate with the nonlinear model.

noise parameters: We distinguish two noice sources: sensor noise and exogeneous forces on the pendulum. We assume that we have an accurate sensor with only discretization noise.

Reasonably, the used sensor will have a resolution of $0.5mm$. We assume that the movement of the rod will result in a uniform distributed white sensor noise.

It is difficult to estimate a-priory an exogeneous noise signal. Therefore it is irrelevant to introduce this noise.

To identify the pendulum, a PRBNS signal is used as input signal. This signal can be characterized by two parameters: The pulse width and the pulse height. The minimum pulse width determines the bandwidth of the signal and the amplitude is a trade-off between nonlinearity effects for large amplitude and a reasonable sensor Signal to Noise Ratio for small amplitude. The input signal and its spectrum are shown in figure 5.1. The chosen input signal has a pulse width of $0.2s$ and an amplitude of $1cm$.

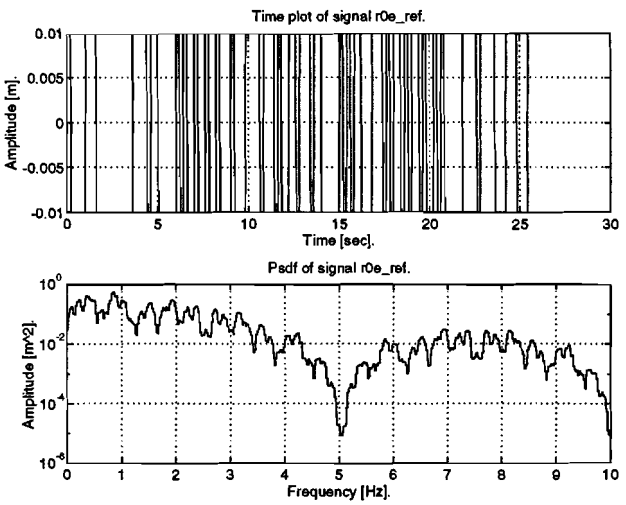

Figure 5.1: *PRBNS Input signal.*

The next design parameters are the sample time and the experiment duration. For convenience the identification sample time is chosen equal to the regulator sample time: 0.05s. For the experiment duration, a rule of thumb is to choose the experiment time $5 - 10$ times the largest time constant of the proces. The largest time constant is in our case the flexible mode time constant, which is $\pm 0.6s$. This results in an experiment duration of $6s$ or $6s \cdot 20Hz \approx 120$ samples. However, because this time constant is very uncertain, we will choose a much longer experiment duration of $25.5s$ or 512 samples.

Every experiment data set includes both an estimation set and a validation set. Because of zero-initial conditions, we will not execute one experiment and split the data in two sets, but execute two different simulations with different input signals. The experiment setup is shown in figure 5.2. The experiment contains 4 exogene signals. `bin_e` is the PRBNS input signal, `noise_e` is the sensor noise and `acc.phi_1 noise` and `acc.phi_2 noise` are disturbances on $\ddot{\varphi}_1$ and $\ddot{\varphi}_2$.

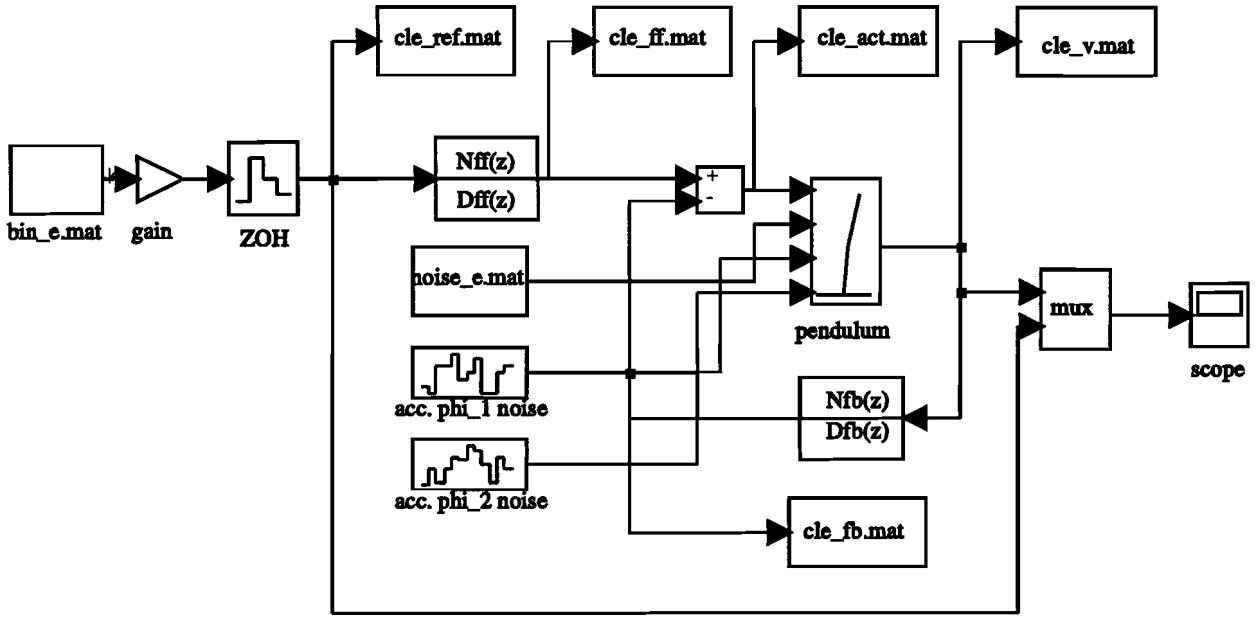

Figure 5.2: *Experiment scheme.*

5.3 The identification method

For identifying the pendulum, an output error model will be used. This is depicted in figure 5.3
The output error model can be written as:

$$y(t) = \hat{y}(t) + \epsilon(t) = \frac{B(z^{-1})}{F(z^{-1})}\tilde{u}(t - t_d) + \epsilon(t), \tag{5.1}$$

$$B(z^{-1}) = b_1 + b_2 z^{-1} + \cdots + b_{n_b} z^{-n_b+1}, \tag{5.2}$$

$$F(z^{-1}) = 1 + f_1 z^{-1} + \cdots + f_{n_f} z^{-n_f}. \tag{5.3}$$

The model parameters $[b_1, \cdots, b_{n_b}]$ and $[f_1, \cdots, f_{n_f}]$ are collected in vector $\underline{\theta}$ and the estimated output error model $\underline{\hat{\theta}}$ is defined as:

$$\underline{\hat{\theta}} = \arg\min_{\underline{\theta}} \frac{1}{N}\sum_{t=0}^{N-1}(y(t) - \hat{y}(t))^2 = \arg\min_{\underline{\theta}} \frac{1}{N}\sum_{t=0}^{N-1}\epsilon^2 = \arg\min_{\underline{\theta}} J_e. \tag{5.4}$$

Here J_e is the loss function of the model. This SISO nonlinear minimalization procedure is performed by the OE.m function of the MATLAB identification toolbox.

To determine the order n_f of the model, figure 5.4 depicts the loss function J_e as function of the order n_f. Based on physical considerations, the delay time t_d is chosen 0. The nonlinear model contains no time delays. The order b_f of the model is determined by trial and error. This order is chosen to minimalize J_e for a given order n_f.

Both loss functions are monotonously decreasing functions. The loss function of the classical designed controller is about an order smaller than the loss function of the H_∞ designed controller.

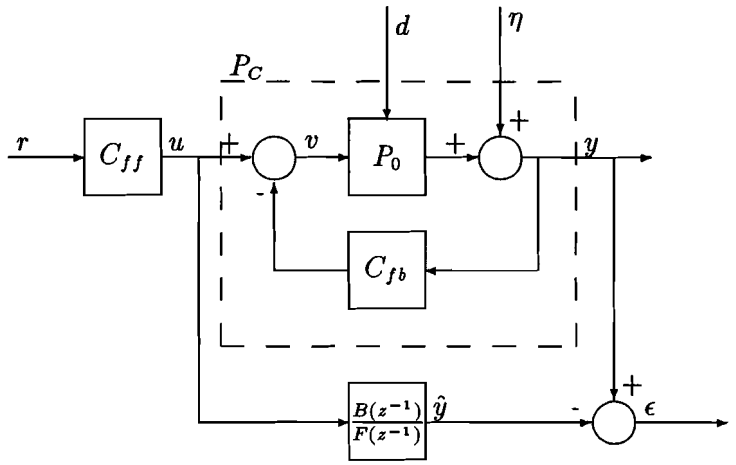

Figure 5.3: *OE model.*

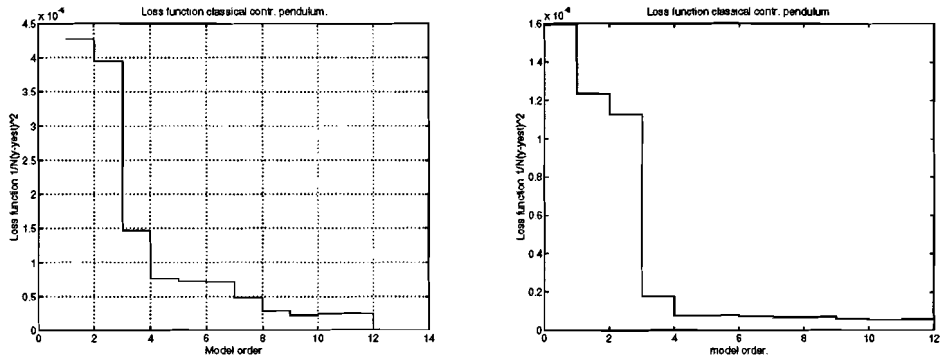

Figure 5.4: *Loss functions H_∞ contr. (left) and classical contr. (right) pendulum.*

The following model order is chosen for the classical controlled model:

$$[n_f, n_b, t_d] = [4, 4, 0],$$

and for the H_∞ controlled model

$$[n_f, n_b, t_d] = [4, 4, 0].$$

This results in the models of figure 5.5 and figure 5.6.

5.4 Model validation.

In the previous section a model is obtained based on the estimation data set. In this section, we will validate these models with the validation data set and accept or reject the presented models.

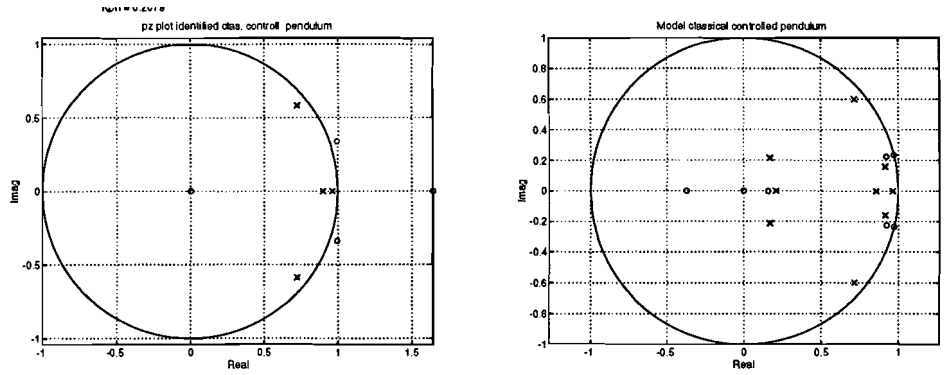

Figure 5.5: *Identified model (left) and linear simulation model (right) classical controlled pendulum.*

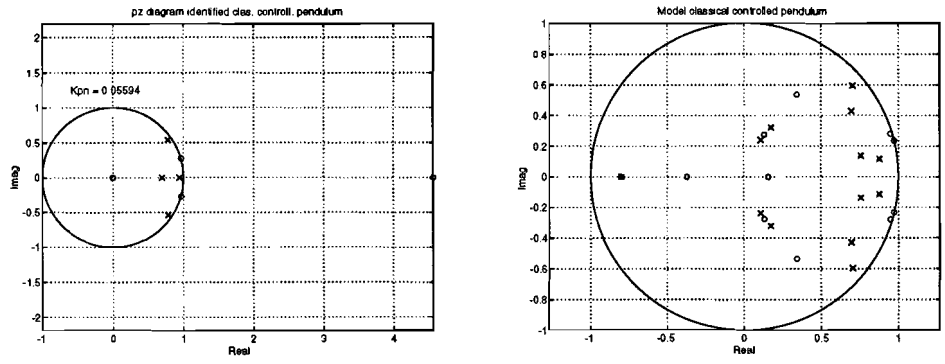

Figure 5.6: *Identified model (left) and linear simulation model (right) H_∞ controlled pendulum.*

An important method for validating the model is checking if a relation can be found between the input signal and the residuals. To test the independence of u and ϵ, we proceed as explained in Bosch [3]. If u and ϵ are indeed independent, we have that

$$\sqrt{N} R_{\epsilon u}(\tau) \in A_s \mathcal{N}(0, P), \tag{5.5}$$

where $A_s\mathcal{N}(0,P)$ means that the given quantity asymptotically converges in distribution to the normal distribution, with mean 0 and variance P. Further on N_α is used as the α level of the $\mathcal{N}(0,P)$ distribution and $R_{\epsilon u}$ is the cross covariance between ϵ and u. P Is defined as

$$P = \sum_{t=-\infty}^{\infty} R_\epsilon(t) R_u(t). \tag{5.6}$$

Here R_u and R_ϵ are the covariance functions of u and ϵ.
It is stated that the input and the residuals are independent if

$$\left|\frac{R_{eu}(\tau)}{\sqrt{R_\epsilon(0)R_u(0)}}\right| \leq \sqrt{\frac{P}{NR_\epsilon(0)R_u(0)}}N_\alpha. \tag{5.7}$$

To evaluate the models, the normalized cross-covariance function of input and residuals is plotted in figure 5.7 and figure 5.8, together with the confidence levels. The associated confidence level used here is $N_{0.01} = 2.58$. This means that we have 99% confidence that the model is good. In this way it is easily seen that both models satisfy condition 5.7. From these figures we can see also a correlation between $\epsilon(t)$ and $u(t-\tau)$ for negative values of τ. In general, this indicates the presence of feedback. This is obviously the case for our model.

The figures also show the auto-covariance of ϵ and a 95% confidence interval that the signal is white. We conclude from this that the residual is certainly not white.

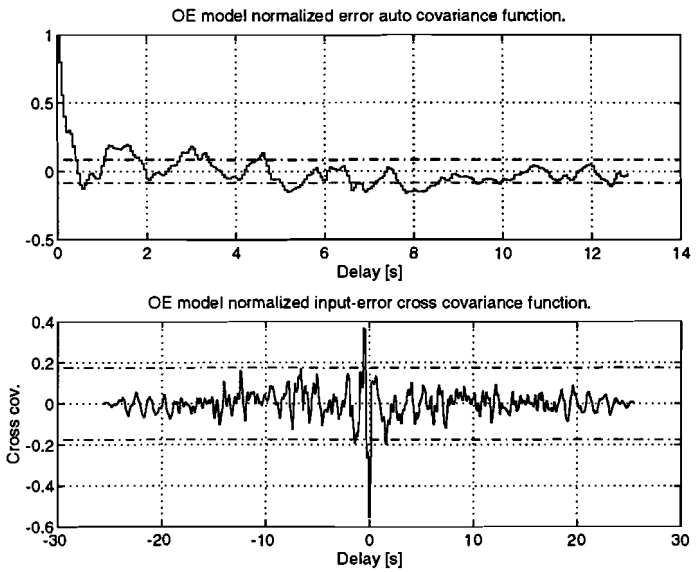

Figure 5.7: *Auto correlation residual signal and cross correlation between input-residual signals of the classical controlled pendulum.*

Finally the estimated output signals are shown in figure 5.9 and figure 6.6. These figures also show the spectra of the residuals. For the classical designed controller, the residuals have a large amplitude for low frequencies. This can be explained by the large complementary sensitivity for low frequencies of this design. This complementary sensitivity is shown in figure 4.9.

The psdf of the residuals of the robust design is relatively large by frequencies around $1Hz$. It seems that the algorithm encouters difficulties by modelling the pole-zero configuration of the closed loop system around this frequency.

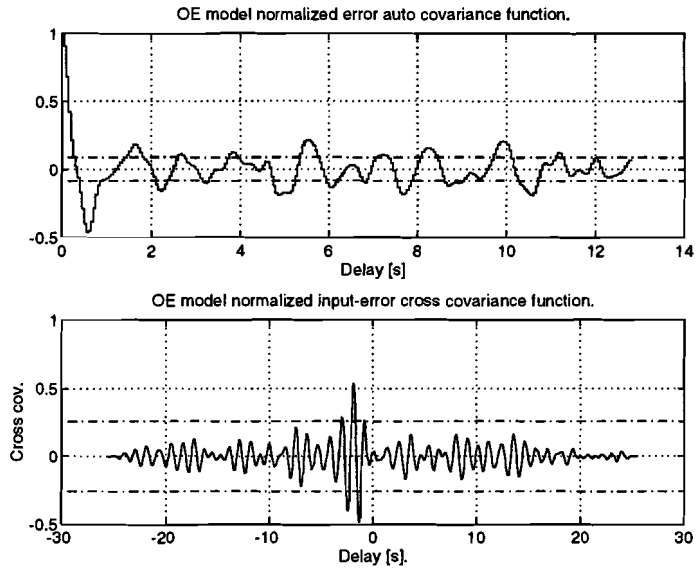

Figure 5.8: *Auto correlation residual signal and cross correlation between input-residual signals of the H_∞ controlled pendulum.*

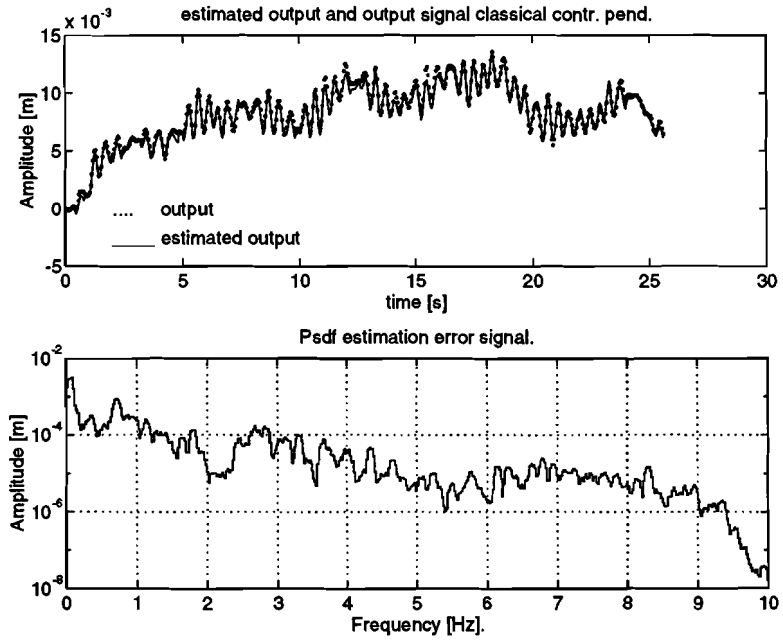

Figure 5.9: *Estimated output signal and psdf of the error signal of the classical controlled pendulum.*

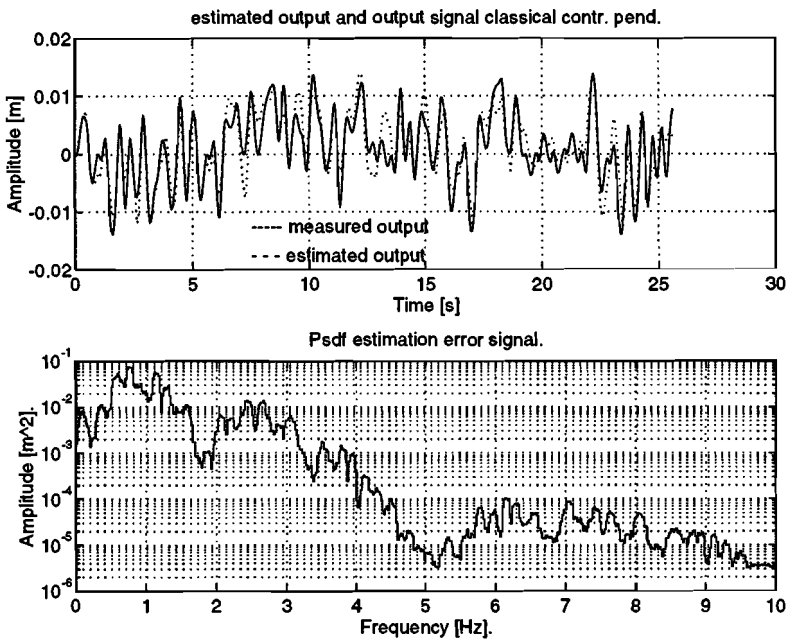

Figure 5.10: *Estimated output signal and psdf of the error signal of the H_∞ controlled pendulum.*

Chapter 6

Second loop controller

6.1 Introduction

In this section the two-loop control design is applied on the inverted pendulum. The design procedure is depicted in figure 6.1. First we have to find the model of the system with a simulation and a identification procedure. Based on this model a robust H_∞ controller is designed and with the updating mechanism a new controller is constructed. If the controller is not significantly changed, the two-loop control design is finished. Otherwise a new iteration can be performed. The simulation and identification blocks are already discussed in the previous chapter. In this chapter we will confine ourselves in the controller design and the update mechanism. These will be discussed with the first iteration step of the initially H_∞ controlled pendulum. Finally the results of the two-loop control will be discussed.

6.2 Robust design procedure

In chapter 4 we have concentrated the design on the robustness properties of the controller, while in this section the performance of the controller is emphasized. The design is based on the robust model obtained in the previous chapter.

The design of the weighting filter is divided in two parts. First the general shape and the order of the weighting filters are derived. The goal of this part is to reduce the number of free parameters in the second part of the design. This part is concerned with the optimalization of the performance.

We will start with the design of the input shaping filters V_d and V_r. Figure 6.2 shows the power spectral density functions of the reference signal and the output disturbance of the first identification procedure. In future identification procedures, we will use the same reference signal. V_r is now chosen as the upper bound of the psdf of the reference signal. For V_d however, if a new controller is designed, the output disturbance will not remain the same because the ouput disturbance is dependent on the used controller. To simplify the controller design we will assume that the new controller will only affect the output noise level, but the shape of the psdf will remain the same.

$$V_d = K_d \frac{(s+0.06)}{(s+5)}, \tag{6.1}$$

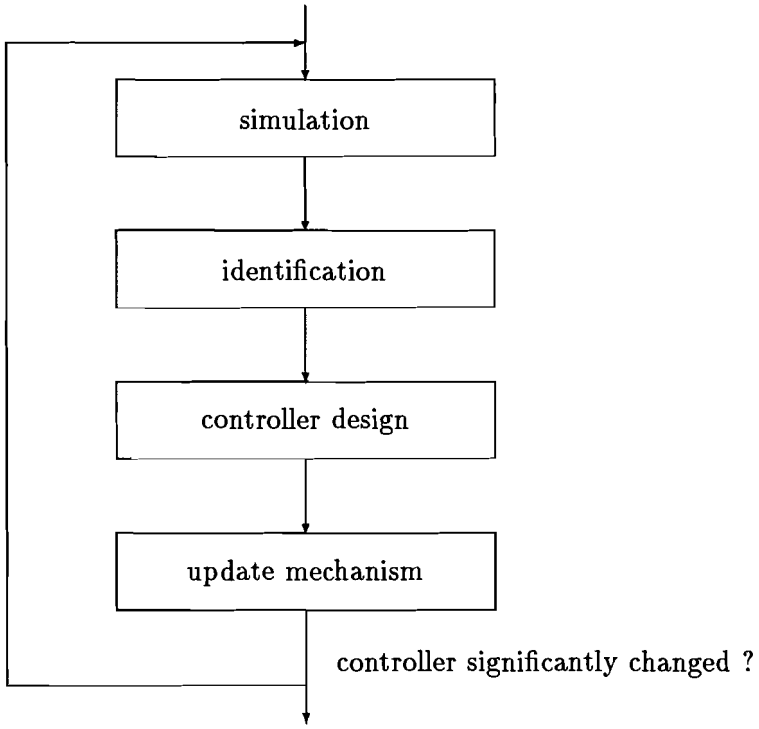

Figure 6.1: *Two loop design.*

$$V_r = 0.125\frac{(s+40)}{(s+10)}. \tag{6.2}$$

Next, W_e is designed. W_e specifies the performance of the system. After some trial and error we will choose for a critical damped second order filter

$$W_e = K_e\frac{s^2+\sqrt{2}\omega_e s+\omega_e^2}{s^2+\sqrt{2}0.1s+0.1^2}. \tag{6.3}$$

The frequency in the denominator is chosen 'small' and the optimization uses 2 degrees of freedom (K_e and ω_e).

Next W_u is designed. This filter determines the model robustness and the actuator saturation. The shape of W_u is chosen to optimize the model robustness. The robust design is based on an additive model perturbation. Based on the identification procedure, it is possible to estimate this additive model perturbation. This perturbation is shown in figure 6.3.

The estimation of the additive model perturbation $|\Delta_P(\omega)|$ can be found with:

$$\Phi_e = \Phi_d + \Phi_u|\Delta_P(\omega)|^2, \tag{6.4}$$

$$|\Delta_P(\omega)| = \sqrt{\frac{\Phi_e-\Phi_d}{\Phi_u}}. \tag{6.5}$$

Here Φ_d is the spectral density function of an independent exogene output disturbance, Φ_e is the psdf of the estimation error signal and Φ_u is the psdf of the input signal of P_C. The

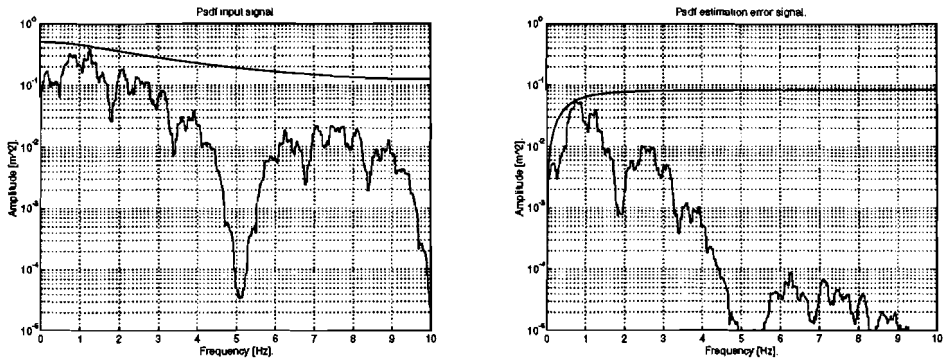

Figure 6.2: *Psdf reference signal (left) and error signal (right) with their upper bounds.*

ω_e	K_e	K_u	K_d	γ
3	50	140	0.05	42

Table 6.1: *Parameters weighting filters.*

spectral density functions Φ_u and Φ_e are obtained in the identification procedure and Φ_d is unknown. If Φ_d is chosen zero, $|\Delta_P(\omega)|$ can be estimated as

$$|\hat{\Delta}_P(\omega)| = \sqrt{\frac{\Phi_e}{\Phi_u}}. \tag{6.6}$$

A nonzero Φ_d will result in a more conservative additive perturbation estimation.

The estimated additive perturbation $|\hat{\Delta}_P(\omega)|$ and the real linear additive perturbation $|\Delta_P(\omega)| = |P_C - \hat{P_C}|$ can be found in figure 6.3. W_u is chosen as a 3rd order filter to obtain a small transition interval at $2Hz$.

$$W_u = K_u \frac{s^3 + 2 \cdot 6.9 \cdot s^2 + 2 \cdot 6.9^2 \cdot s + 6.9^3}{s^3 + 2 \cdot 15 \cdot s^2 + 2 \cdot 15^2 \cdot s + 15^3}. \tag{6.7}$$

The only degree of freedom of this filter is K_u.

We have now defined the weighting filters and the filter parameters to optimize the performance. With parameter ω_e the bandwidth of the system can be adjusted. However, if ω_e is chosen too high, the robustness demands of figure 6.3 is violated. The ratio between K_u and K_e is used to adjust the actuator saturation and finally the absolute gains K_u, K_e and K_d are mainly used to avoid numerical problems. After some trial and error, the final paramater values can be found in table 6.2.

These weighting filters results in the transfer functions of figure 6.4. Note that the x-axis of these figures are relative frequencies of the fundamental interval, with a sample frequency of 20Hz. Although the filter design is performed in the continous-time domain, the controller calculation is performed in the discrete-time domain.

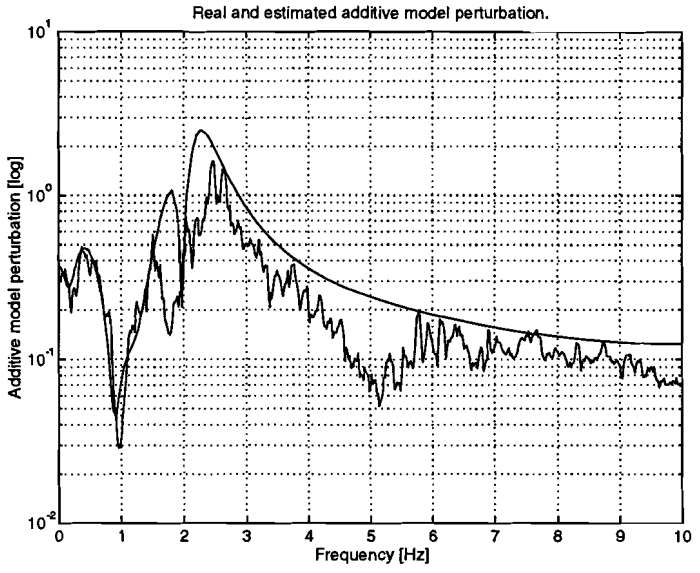

Figure 6.3: *Real and estimated additive model perturbation.*

6.3 Updating mechanism

Figure 1.4 shows that updating the controllers consist of adding the feedback controllers and cascading the feedforward controllers. However the feedforward controller of the H_∞ design has as input the reference signal. In this way, the former feedforward controller has become superfluous and the total feedforward controller can be directly obtained by the H_∞ design.

Because C and ΔC do not have the same poles, the order of the controller will increase with every iteration step. It is obvious that each iteration the order of the controller has to be reduced.

For reducing the order of the controller, we will use a time-domain approach. The two controllers are added and the matching impulse response is determined. Based on this impulse response, a new controller is estimated. For estimating this controller, the Steiglitz-McBride algorithm is used. This is a nonlinear least square estimation algorithm, which minimalizes the error between a given impulse response and the impulse response of the estimated transfer function in a least square sense.

Not only the order of the feedback controller has to be reduced, but also the order of the feedforward controller. For this purpose, the same algorithm is used. The results of the order reduction are shown in table 6.3 and table 6.3.

These tables shows the power of the estimation error, the Signal to Noise Ratio of the estimation error power and the impulse response power and the absolute maximum difference between the real and the estimated impulse response respectively. Based on these tables, the order of the feedforward controller is chosen 5 and the order of the feedback controller 6.

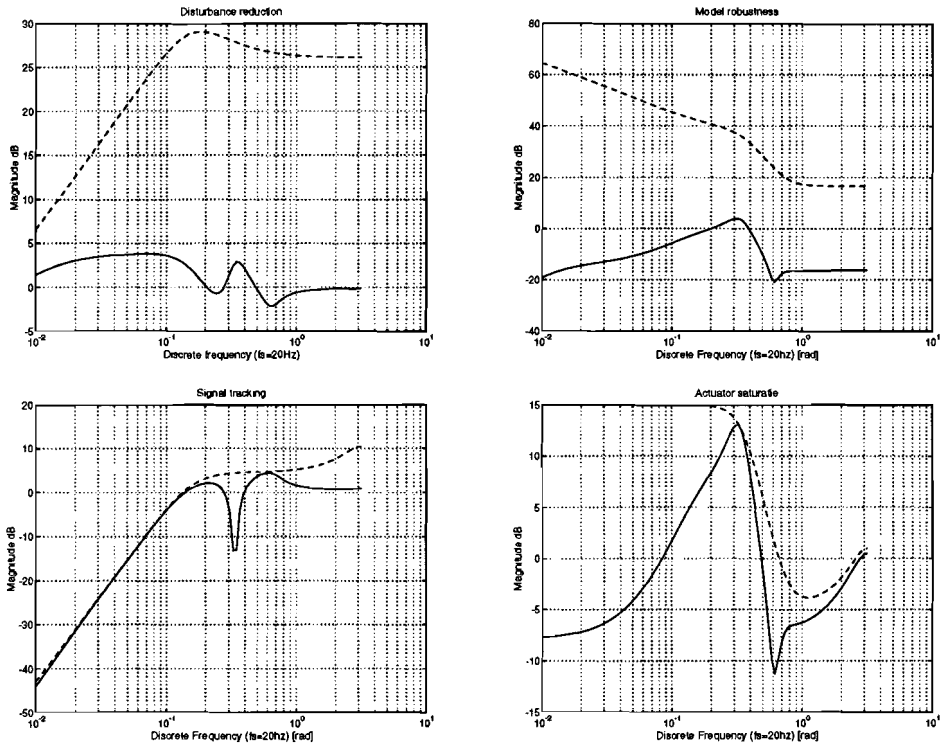

Figure 6.4: *Transfer functions with robust controller.*

order	J_{error}	SNR	$max\|h - \hat{h}\|$
1	4.7836e-002	1.1105e+000	6.7847e-001
2	1.2454e-003	4.2654e+001	4.4108e-001
3	1.1926e-003	4.4545e+001	4.2404e-001
4	4.6445e-004	1.1438e+002	2.1587e-001
5	2.8654e-004	1.8539e+002	1.1956e-001
6	1.9555e-005	2.7165e+003	2.3731e-002
7	1.9511e-005	2.7227e+003	2.3006e-002
8	6.1503e-006	8.6373e+003	1.3052e-002
9	3.3973e-006	1.5637e+004	1.0767e-002

Table 6.2: *feedback controller order reduction.*

order	J_{error}	SNR	$max\|h - \hat{h}\|$
1	1.0327e-003	2.2094e+000	2.1385e-001
2	5.9287e-004	3.8484e+000	1.3594e-001
3	2.4840e-004	9.1852e+000	1.2294e-001
4	1.9139e-004	1.1921e+001	8.0099e-002
5	2.4281e-006	9.3968e+002	8.3535e-003
6	2.1490e-006	1.0617e+003	8.8601e-003
7	8.1211e-008	2.8095e+004	8.1278e-004
8	2.1333e-009	1.0695e+006	3.5779e-004
9	3.2610e-015	6.9967e+011	5.5337e-007

Table 6.3: *feedforward controller order reduction.*

6.4 Simulation results

Two evaluate the two-loop control, figure 6.5 shows the impulse responses of the updated controller after 1 iteration and figure 6.7 shows the impulse responses after 2 iterations. These figures also show the impulse response of the added feedback controller ΔC_{fb}. It can be observed that ΔC_{fb} of the 2nd iteration is smaller than the 1st iteration and it seems that the feedback controller will converge to a final controller.

Figure 6.6 and 6.8 show the output signal and the psdf of the model error signal after 1 and 2 iterations respectively. These figures show that the model error has become worse and therefore a more robust controller has to be designed to ensure stability. So the two loop designed controller will not converge to an optimal controller.

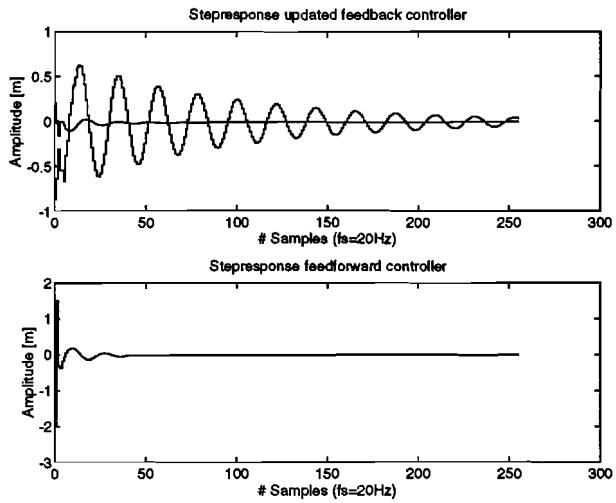

Figure 6.5: *Impulse response feedback and update feedback controller and impulse response feedforward controller (1st two-loop iteration).*

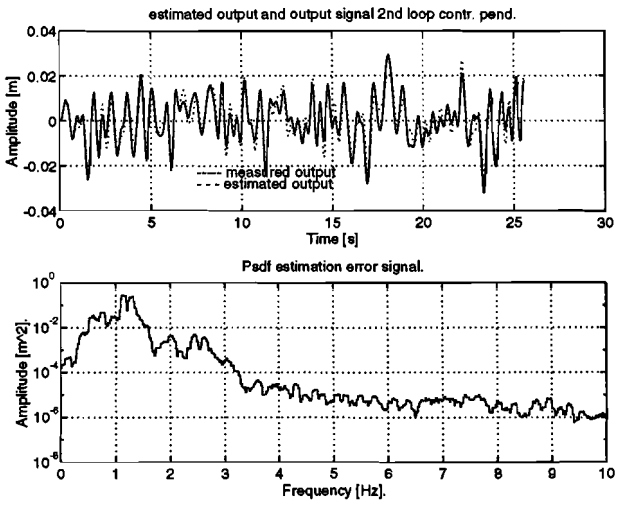

Figure 6.6: *Output signal and psdf estimation error signal (1st two-loop iteration).*

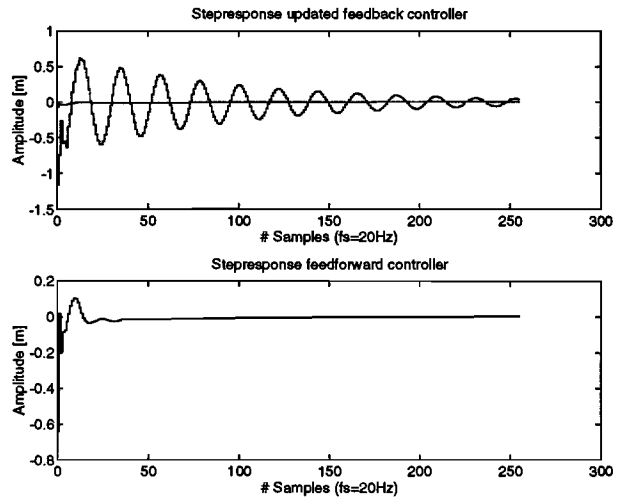

Figure 6.7: *Impulse response feedback and update feedback controller and impulse response feedforward controller (2nd two-loop iteration).*

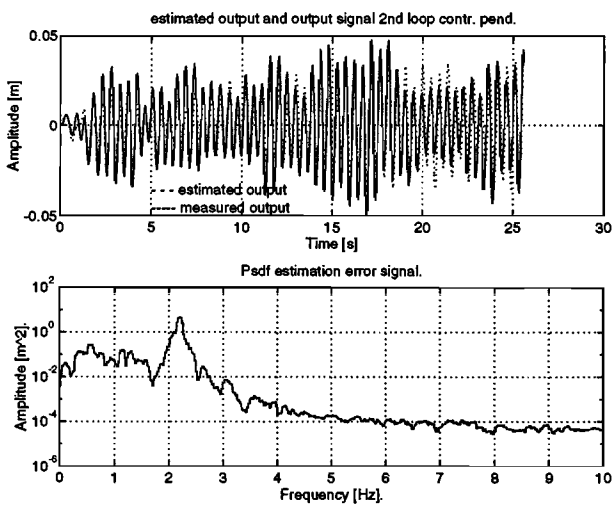

Figure 6.8: *Output signal and psdf estimation error signal (2nd two-loop iteration).*

Chapter 7

Conclusions and recommendations

With a H_∞ robust control technique and the two-loop control structure, we have tried to optimize the performance. The design consists of two parts.

The first part is focused on robustly stabilizing the pendulum, with respect of the flexible mode frequency. The H_∞ is compared with a classical pole zero cancellation design. The flexible mode frequency robustness of both controllers are approximately the same.

The second part consist of an iteratively identification and control design procedure. Because of identification problems, the stabilized pendulum, the algorithm will not converge to controller with optimal performance.

For further survey of the pendulum, the identification problems of the pendulum could be more accurately investigated.

Bibliography

[1] Backx, A.C.P.M. and A.J.W. Boom van den
Toegepaste systeemtheory.
Eindhoven, Technische Universiteit Eindhoven, 1993, Dictaatnr. 5770.

[2] Belt H.J.W.
Two-loop adaptive control with open-loop identification Eindhoven, Section ER, Faculty of electrical engineering, Eindhoven University of technology, 1993
M. Sc. Theses

[3] Bosch P.
Stochastische systeemtheorie.
Eindhoven, Technische Universiteit Eindhoven, 1993.

[4] Cannon R.H. and D.F. Rosenthal
Experiments in control of flexible structures with noncollocated sensors and actuators.
J. of Guidance, Control and dynamics, Vol.7(1984), p.546-553.

[5] Damen A.A.H. and H.H. Ven van de
Moderne regeltechniek.
Eindhoven, Technische Universiteit Eindhoven, 1992, Dictaatnr. 5662.

[6] Falkus H.M.
H_∞ Robust control design for an electromechanical servo system.
Eindhoven, Technische Universiteit Eindhoven, 1990. M. Sc. Thesis

[7] Freriks L.W.
Implementatie en realisatie van onderdelen van een geinverteerd pendulumsysteem.
Eindhoven, Technische Universiteit Eindhoven, 1991.

[8] Glover K. and J.C. Doyle
State-space formulae for all stabilizing controllers that satisfy an H_∞ - norm bound and relations to risk sensitivity.
Systems and Control Letters, Vol. 11, 1988, pp 167-172.

[9] Kawaji Shigeyasu and Kazunobu Kanazawa
Control of Double Inverted Pendulum with Elastic Joint.
In: Proceedings IROS '91. IEEE/RSJ International Workshop on Intelligent Robots and Systems '91. Intelligence for Mechanical systems, Osaka, Japan, 3-5 Nov. 1991. New York, NY, USA: IEEE, 1991. Vol. 2, p.946-951.

[10] Kylstra, F.J.
Robotbesturing.
Eindhoven, Technische Universiteit Eindhoven, 1990, Dictaatnr. 5733.

[11] Lindler D.K. and K.M. Reichard, L.M. Tarkenton
Zeros of modals of flexible structures.
IEEE Transactions on Automatic Control, Vol.38(1993), p.1384-1388.

[12] Simons W.F.J.
Two-loop static state feedback for the mimo gantry crane.
Eindhoven, Technische Universiteit Eindhoven, 1993. M. Sc. Theses

[13] Vidyasagar, H.
Control systems synthesis: A factorization approach
M.I.T. press, 1985

[14] Williams T
Transmission-zero bounds for large space structures, with applications.
J. of Guidance, Control, and Dynamics, Vol.12(1989), p.33-38.

[15] Zhu, Y.C. and M.H. Driessen, A.A.H. Damen, P. Eykhoff
A new scheme for identification and control
Eindhoven, Faculty of electrical engineering, Eindhoven University of technology, 1988
EUT Report 88-E-213

Appendix A

List of symbols

α	Standard problem.	
$A,\ B,\ C,\ D,\ E$	Linear state-space model pendulum.	
$\beta_d,\ \tilde{\beta}_d,\ \Delta\beta_d$	Flexible mode pole (damping, perturbed damping and relative damping).	$[rads^-$
$\beta_n,\ \tilde{\beta}_n,\ \Delta\beta_n$	Flexible mode zero (damping, perturbed damping and relative damping).	
β_r	Relative damping xy-recorder.	
$B(z^{-1}),\ b_i$	Numerator polynomial and polynomial coefficients estimated model.	
$C,\ C_{ff},\ C_{fb}$	General, feedforward and feedback controller.	
C_{st}	Stabilizing controller.	
$c_1,\ c_2$	Friction constant.	$[Nms]$
$\Delta C,\ \Delta C_{ff},\ \Delta C_{fb}$	General, feedforward and feedback update controller.	
$\Delta_N,\ \Delta_M$	Stable factor perturbations.	
$\Delta_n,\ \Delta_d$	Perturbation in numerator and denominator model.	
$\Delta_p,\ \hat{\Delta}_p$	Additive perturbation and estimated additive perturbation.	
D	Loss energy pendulum.	$[Nm]$
d	Output disturbance signal pendulum.	
$\underline{d}$	Output disturbance vector.	
d_f	Stable polynomial.	
$d_N,\ d_M$	Denominator stable coprime factors.	
$d_{nf},\ \tilde{d}_{nf}$	Denominator polynomial not belonging to the flexible mode.	
η	Sensor noise signal.	
$\underline{\eta}$	Sensor noise vector.	
ϵ	Estimation error signal.	
$E(\underline{x}),\ \underline{f}(\underline{x}),\ \underline{g}(\underline{x}),\ \underline{h}(\underline{x})$	Nonlinear state-space model.	
$\tilde{e}$	Augmented plant error signal.	
$F(z^{-1}),\ f_i$	Denominator polynomial and polynomial coefficients estimated model.	
f	Actuator force.	$[N]$
$\underline{f}_l$	Force/torque input vector.	
γ	Scaling factor state-space approach.	
G	Augmented plant.	
$G_{11},\ G_{12},\ G_{21},\ G_{22}$	Partitioned augmented plant.	
g	Gravity force.	$[ms^{-2}]$

H	Sensor height.	$[m]$
$J_1,\ J_2$	Inertia lower and upper rod of the IP.	$[kgm^2]$
J_e	Loss function.	
K	Spring constant.	$[Nm]$
$K_d,\ K_e,\ K_r,\ K_u$	Gain weighting and shaping filters.	
$K_l,\ K_h$	Lower and upper controller gain stability boundary.	
L	Length lower pendulum rod.	$[m]$
$l_1,\ l_2$	Distance joints to center of mass rods IP.	$[m]$
M_C	Optimization function.	
M_{11}	Disturbance reduction criterion.	
M_{12}	Signal tracking criterion.	
M_{21}	Model robustness criterion.	
M_{22}	Actuator saturation criterion.	
M_{11}^*	Disturbance reduction.	
M_{12}^*	Signal tracking.	
M_{21}^*	Model robustness.	
M_{22}^*	Actuator saturation.	
$m_1,\ m_2,\ M$	Masses of lower and upper rod of the IP and cart.	$[kg]$
N	Number of samples.	
N_α	α level normal distribution.	
n_0	Numerator polynomial of the nominal model.	
$n_b,\ n_f$	Order numerator, denominator output error model.	
$n_r,\ n_d$	Reference and disturbance signal augmented plant.	
$n_{nf},\ \tilde{n}_{nf}$	Numerator polynomial not belonging to the flexible mode.	
P	Variance of the normal distribution.	
$\Phi_d,\ \Phi_e,\ \Phi_u$	Power spectral density functions output disturbance, model error and stabilized pendulum input.	
$\varphi_1,\ \varphi_2$	Angle of joint 1 and joint 2.	$[rad]$
$P_0,\ \tilde{P}_0,\ \hat{P}_0$	Nominal, perturbed and estimated pendulum.	
$P_C,\ \tilde{P}_C,\ \hat{P}_C$	Nominal, perturbed and estimated stabilized pendulum.	
$P_N,\ P_M,\ \tilde{P}_N,\ \tilde{P}_M$	Stable coprime factors and perturbed stable coprime factors.	
$p_d,\ p_e,\ p_r,\ p_u$	Poles weighting and shaping filters.	
$\bar{\sigma}(M_C)$	Largest singular value M_C.	
R_e	Auto-covariance function error signal.	
R_{eu}	Cross-covariance function error-input signal.	
R_u	Auto-covariance function model input signal.	
S	Sensitivity function.	
$\underline{\Theta},\ \underline{\hat{\Theta}}$	Model parameters and estimated model parameters.	
T	Kinetic energy pendulum.	$[Nm]$
U	Potential energy pendulum.	$[Nm]$
U_0	Rest energy spring.	$[Nm]$
$\underline{u}$	Stabilized plant input vector.	
u	Stabilized pendulum input signal.	
$\tilde{u}$	Augmented stabilized plant input signal.	
V_d	Output disturbance shaping filter.	
V_r	Reference shaping filter.	

$\underline{v}$	Input vector plant.	
v	Pendulum actuator signal.	$[m]$
v'	Position arm xy-recorder.	$[m]$
ω_e	Bandwidth tracking error weighting filter.	$[rads^{-}$
$\omega_d,\ \tilde{\omega_d},\ \Delta\omega_d$	Flexible mode pole (frequency, perturbed frequency and relative perturbation).	$[rads^{-}$
$\omega_n,\ \tilde{\omega_n},\ \Delta\omega_n$	Flexible mode zero (frequency, perturbed frequency and relative perturbation).	$[rads^{-}$
ω_r	Bandwidth xy-recorder.	$[rads^{-}$
W_u	Actuator saturation weighting filter.	
W_e	Tracking error weighting filter.	
$W_N,\ W_M$	Weighting filters on stable factor perturbations.	
$\underline{w}$	Exogene input vector (augmented) plant.	
$(x_1, y_1),\ (x_2, y_2)$	Position center of mass lower and upper rod	$[m]$
$\underline{x}_l$	Independent variables pendulum.	
$\underline{y}$	Output vector plant.	$[m]$
$y,\ \hat{y}$	Output and estimated output pendulum.	$[m]$
$\underline{z}$	Output vector augmented plant.	
$z_d,\ z_e,\ z_r,\ z_u$	Zeros weighting and shaping filters.	

Appendix B

The simulink nonlinear model

The functions of the simulink scheme of figure B.1 are defined as:

```
f1(u)=-(m1*l1+m2*L)*u[1]*cos(u[2])-m2*L*l2*sin(u[2]-u[3])*(u[5])^2+...
      (m1*l1+m2*L)*g*sin(u[2])+K*(u[3]-u[2])-c1*u[4]+c2*(u[5]-u[4])
f2(u)=-m2*l2*cos(u[3])*u[1]+m2*l2*L*sin(u[2]-u[3])*u[4]^2+...
      m2*l2*g*sin(u[3])-K*(u[3]-u[2])-c2*(u[5]-u[4])
f3(u)= (m1*l1^2+m2*L^2+J1)*(m2*l2^2+J2)-(m2*L*l2*cos(u[2]-u[3]))^2
f4(u)= (u[1]*(m2*l2^2+J2)-u[2]*m2*L*l2*cos(u[4]-u[5]))/u[3]
f5(u)= ((m1*l1^2+m2*L^2+J1)*u[2]-u[1]*m2*l2*L*cos(u[4]-u[5]))/u[3]
f6(u)=L*sin(u[1])+(H-L*cos(u[1]))*sin(u[2])
```

The functions `f1(u)` and `f2(u)` are parts of the system equation $\underline{f}(\underline{x})$. The inversion of $E(\underline{x})$ is accomplished with functions `f3(u)`, `f4(u)` and `f5(u)`. The output function $\underline{h}(\underline{x})$ is realized with function `f6(u)`.

The following numerical values are used for the physical parameters:

```
g = 9.81;
K = 2;
L = 0.75; H= 1.4;
m1= 0.25; m2=0.25;
c1= 1.03e-2; c2=0.0225;
l1= L/2; l2=L/2;
J1=(m1*L^2)/12; J2=(m2*L^2)/12;
w0=sqrt(50/0.05); % undamped frequency xy-recorder
b=0.82;       % damping ratio xy-recorder
```

Finally, the following noice variances are chosen:

```
acc phi_1 noice : 0
acc phi_2 noice : 0
sensor noice    : Uniform distributed noise between (-0.25mm, 0.25mm)
```

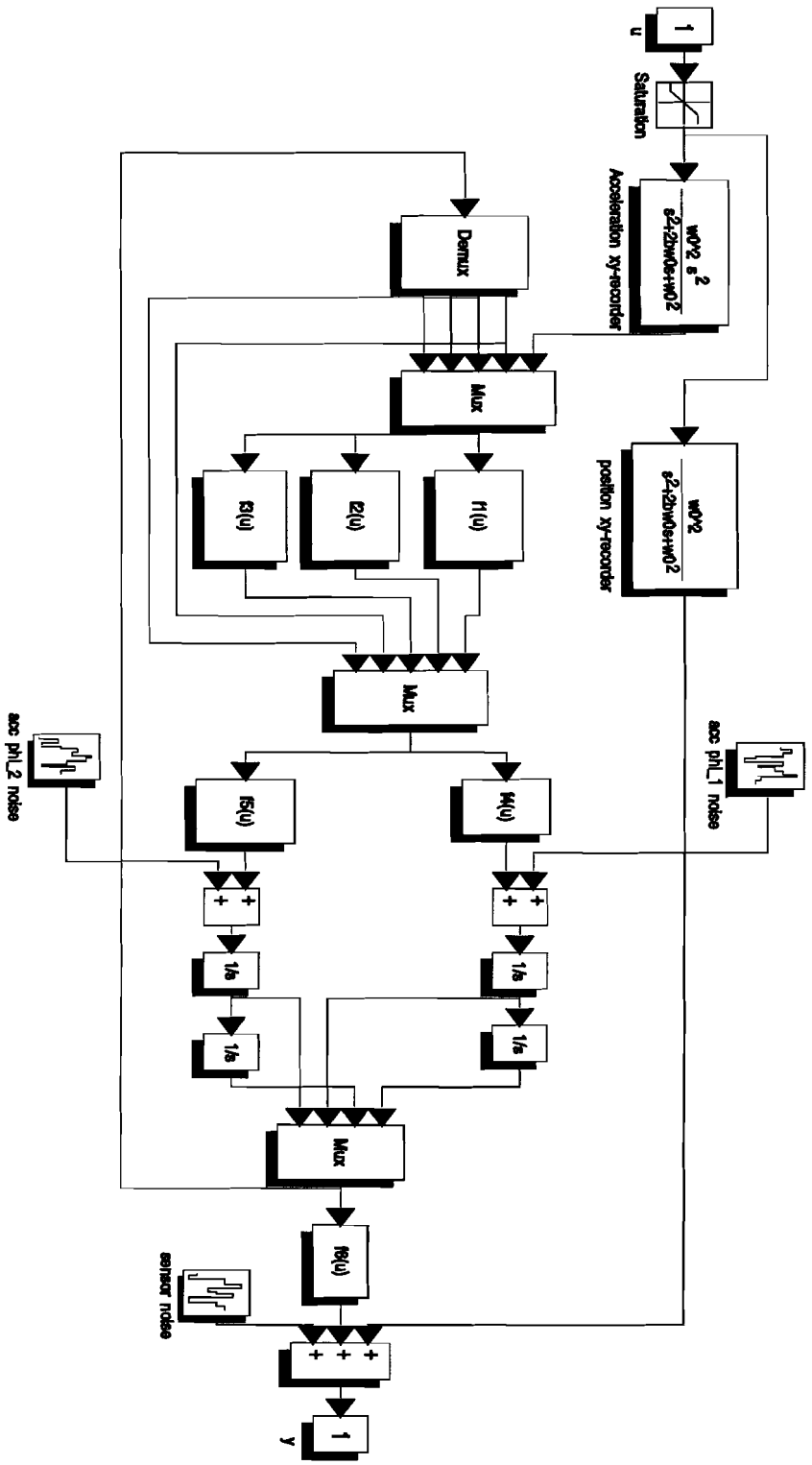

Figure B.1: *Nonlinear simulink scheme of the flexible inverted pendulum.*